Submitted as a Chapter in
"Treatise on Solid State Chemistry",
N. B. Hannay, Ed.

LBL-2257
Preprint c. 1

# THE STRUCTURE AND THERMODYNAMICS OF CLEAN SURFACES-PRINCIPLES

G. A. Somorjai

October 1973

Prepared for the U. S. Atomic Energy Commission
under Contract W-7405-ENG-48

For Reference

Not to be taken from this room

RECEIVED
LAWRENCE
RADIATION LABORATORY

JAN 2 1974

LIBRARY AND
DOCUMENTS SECTION

LBL-2257
c. 1

## DISCLAIMER

This document was prepared as an account of work sponsored by the United States Government. While this document is believed to contain correct information, neither the United States Government nor any agency thereof, nor the Regents of the University of California, nor any of their employees, makes any warranty, express or implied, or assumes any legal responsibility for the accuracy, completeness, or usefulness of any information, apparatus, product, or process disclosed, or represents that its use would not infringe privately owned rights. Reference herein to any specific commercial product, process, or service by its trade name, trademark, manufacturer, or otherwise, does not necessarily constitute or imply its endorsement, recommendation, or favoring by the United States Government or any agency thereof, or the Regents of the University of California. The views and opinions of authors expressed herein do not necessarily state or reflect those of the United States Government or any agency thereof or the Regents of the University of California.

# THE STRUCTURE AND THERMODYNAMICS OF CLEAN SURFACES—PRINCIPLES

G. A. Somorjai

Department of Chemistry, University of California
and Inorganic Materials Research Division, Lawrence Berkeley Laboratory
Berkeley, California 94720

# I. INTRODUCTION

Surfaces, whether we glance at the face of a smiling infant or view the massive steel support of the Golden Gate Bridge, are a part of our everyday life. When there is condensed phase present there are surfaces or as it should be called--there are interfaces. The physical and chemical properties of these interfaces that form between the solid, liquid and gas have been under close scientific scrutiny for some time. Part of the interest stems from our attempt to understand the nature of phase changes that take place at the interface, (growth, vaporization, melting just to mention a few). Over and above our interest in phase changes, the surface has two unique functions that makes its study so important: 1. The surface is the first line of defense of the condensed phase from chemical or mechanical attack. Thus passivation of the surface against such an attack is one of our primary concerns; 2. There are chemical reactions that require much less activation energy when they occur at the surface instead of the gas phase or inside the solid phase. As a result, surface reaction rates are orders of magnitude greater than rates for the same reaction in other phases which makes surface reactions of great industrial and also of great biological importance. Industries like oil, polymer and pharmaceuticals have their technologies firmly based on heterogeneous catalysis, i.e., on reactions at the solid-gas or solid-liquid interface that take place selectively and at optimum rates. Evolution has developed biological systems (bone, brain, membranes) with very large surface-to-volume ratio to optimize chemical reaction rates that are to take place. It is amusing to think of our body as a condensed phase with enormous surface-to-volume ratio.

Our understanding of the physical-chemical properties of surfaces, until recent times, has been poor when compared to our knowledge of these properties for atoms or molecules in the gas phase or in the solid state. The reason for our lack of information about surface properties becomes clear when we compare the density of surface atoms with the density of atoms in the bulk of the solid. A typical solid, like silver, has a bulk density of about $5.9\times10^{22}$ atoms per cubic centimeter. The surface density of atoms can be estimated to be approximately the two-thirds power of the volume density that is equal to $1.5\times10^{15}$ atoms per square centimeter. Thus, in any experiment that is aimed at studying the surface one attempts to investigate the properties of approximately $10^{15}$ atoms per square centimeter in the background of a much larger concentration of bulk atoms. Clearly, we need experimental techniques that are sensitive only to the topmost atomic layer at the interface. In the past, the development of surface science was hampered by the scarcity of experimental tools that provide information about the surface layer only without containing a great deal of bulk information as well. Surface scientists, therefore, were forced to prepare and carry out measurements on samples of high surface-to-volume ratio, i.e., small particles. Since particles of small size are very important in many fields of applied surface science, heterogeneous catalysis, photography, colloid science, most fundamental physical chemical properties of surfaces are naturally studied in this medium. Many ingenious experiments are carried out to determine the particle sizes accurately to measure the amount of gases adsorbed on the surface of the particles and to monitor the rates of chemical reactions that take place. Although studies of the various properties of the clean particle surfaces

are difficult to carry out, a great deal of knowledge of the properties of adsorbed gases and liquids has been accumulated this way.

In spite of the very large efforts of generations of ingenious experimentalists in surface science, there were serious limitations to the investigations of some of the fundamental properties of clean and gas-covered surfaces through studies of such dispersed systems of small particles. The atomic structure of the surface was unknown. Often the surface information that is to be extracted from changes of experimental parameters was only a small fraction of the total change and was of the magnitude of the experimental uncertainty. For example, surface heat capacity measurements using small particles have been attempted by many but succeeded only rarely.

From the middle 1950's, however, there have been several technological developments which brought renewed attention to surfaces and made possible studies of their fundamental physical-chemical properties. Semiconductor devices with large surface-to-volume ratios necessitated a better understanding of the structure and electrical properties of clean surfaces. Single crystals in ultra high purity (impurity concentrations in the parts per billion range) became available in ever increasing numbers and found technological use. Due to efforts of space exploration, modern vacuum technology has developed to unprecedented levels such that the attainment of ultrahigh vacuum (less than $10^{-8}$ Torr) became available at a moderate cost and within reasonable experimental times (hours). The ambient gas flux striking a surface at $10^{-6}$ Torr is large enough (approximately $10^{15}$ molecules/cm$^2$/second) to cover a surface of typical atomic density if every molecule incident on the surface sticks. At $10^{-8}$ Torr there is at least $10^2$ seconds available before a monolayer adsorbs on the surface. Thus, the attainment of ultrahigh vacuum made the study of clean surfaces possible for the first time.

Before the advent of ultrahigh vacuum technology most of the surface experiments were concentrating on the properties of the adsorbed layer. Physical adsorption and chemical adsorption (or chemisorption as it is commonly called) will be the subject of one of the chapters. However, experiments can now be carried out with surfaces initially in vacuum with all of the gas atoms removed and one may determine the properties of surface atoms before and during adsorption. It became clear that studies of the fundamental properties of surfaces should be carried out, whenever possible, on initially clean and preferably single crystal surfaces. Experimental evidence began to accumulate indicating that the atomic structure of the surface is an important variable in the determination of the reactivity of surfaces. Today, surface studies can be carried out on one face of a crystal in ultrahigh vacuum with relative ease.

Many new experimental techniques have become available in recent years that can be applied to the studies of clean surfaces and to studies of the properties of the solid-gas interface (for example, low energy electron diffraction, Auger electron spectroscopy, ellipsometry, atomic beam scattering, etc. These will be discussed in detail in the next chapter. As a consequence, the physical-chemical properties of surfaces in vacuum and of the solid-gas interface are being uncovered at an unprecedented rate. Unfortunately, most of these techniques are not applicable to studies of solid-liquid interfaces. Solids and liquids are of about equal atomic density and it is difficult to find techniques that may penetrate one phase without penetrating the other and thereby provide information about the interface. Indeed, the solid-liquid interface is still one of the frontier areas of surface science that awaits further experimental innovations. Thus, we shall concentrate on describing

the physical-chemical properties of surfaces in vacuum and properties at the solid-gas interface. This is the area of surface science that much of our understanding of surfaces has been accumulating in recent years.

In studies of surfaces we would like to rely on knowing two fundamental properties. These are:

1. The thermodynamic properties of surfaces. Thermodynamic studies allow us to determine which crystal faces of solids would be likely to form in a variety of conditions. From the surface thermodynamic properties, we should be able to predict the surface composition of multicomponent systems (alloys for example) and changes of surface free energy upon adsorption, adhesion, or lubrication.
2. The structure of the surface. The determination of the atomic surface structure is just as important as determination of the structure of solids by x-ray diffraction.

We wish to know these fundamental properties for the clean surface and for the adsorbed layer as well. With the atomic surface structure and thermodynamic properties in hand we are in a good position to investigate the dynamical properties of surfaces which include atom transport and the transport of charges (electron and ions) along surfaces. All of these properties are to be considered and taken into account in studies of more complex surface chemical reactions that so frequently occur in biochemical systems and in chemical technologies that employ heterogeneous catalysis.

In this chapter, we shall discuss solely the thermodynamics and the atomic structure. Detailed description of the physical-chemical properties of the adsorbed layer and the techniques that are used in surface studies will be discussed in the chapters that follow.

## THERMODYNAMICS OF SURFACES

The thermodynamic parameters that are used to characterize the surface are defined separately from the bulk thermodynamic parameters that characterize the homogeneous phase.[1-3] The specific surface energy $E^s$, the energy per surface atom, is related to the total energy of the condensed phase E by the relation

$$E = NE^o + AE^s \tag{1}$$

where A is the surface area of a solid which is comprised of N atoms, and $E^o$ is the energy of the condensed phase per atom. Thus, $E^s$ is the specific surface energy, or excess energy the solid has over $E^o$ which is the energy it would have if the surface were in the same thermodynamic state as the isotropic interior. The other surface thermodynamic functions such as the specific surface free energy, $G^s$, specific surface entropy $S^s$, and specific surface enthalpy $H^s$, are defined the same way as $E^s$ in Eq. 1. The surface thermodynamic functions are related by equations that are identical to those relating the bulk thermodynamic functions. For example,

$$G^s = H^s - TS^s \tag{2}$$

$$\left(\frac{\partial G^s}{\partial T}\right)_P = -S^s \tag{3}$$

If we create more surface by increasing the surface area, the surface work, $\delta W^s$, at a constant temperature, T and pressure P is given by Eq. 4.

$$\delta W^s = d(G^s A) \tag{4}$$

If $G^s$ is independent of the surface area, surface work is

$$\delta W^s = G^s dA \tag{5}$$

For a one-component system the specific surface free energy, $G^s$, is frequently called the surface tension, or the surface pressure and denoted by $\gamma$ ($G^s = \gamma$). $G^s$ or $\gamma$ maybe viewed as a pressure applied along the surface. The surface pressure has dimensions of force per unit length (dynes/centimeter or Newton/meter). The customary units of the surface tension, ergs/cm$^2$ or dyne/cm are dimensionally identical. It should be noted that more surface may be created by stretching the existing surface without changing the number of surface atoms. The strain energy however, is neglected in our treatment. There are textbooks that may be consulted for more detailed discussion of surface thermodynamic parameters.

Creation of a surface or more surface always has positive free energy change associated with it. Thus, creating more surface requires work and increases the total free energy of the system. In order to minimize their free energy, solids or liquids assume shapes, in equilibrium, with the minimum exposed surface area possible. Since the specific surface free-energy or surface tension is one of the most important thermodynamic parameters characterizing the condensed phase, its measurement is of great importance. The various methods of surface free-energy measurements are described elsewhere.[4,5] In Table 1 we list the experimentally determined surface tensions of selected nonmetallic solids and liquids and the temperature where these values were measured. It is, in general, easier to measure the surface tension of liquids and a great variety of reliable techniques are available for this purpose. However, it would be of great value to be able to estimate $\gamma$ for various solids and liquids where such measurements are less reliable. Such estimates are available for metals[6] and these will be discussed below.

The surface free energy is temperature dependent according to Eq. 3 and from its temperature dependence the specific surface entropy may be determined. A semiempirical equation for predicting the temperature dependese of $\gamma$ is

$$\gamma = \gamma^{o}(1 - T/T_c)^n \tag{6}$$

where $T_c$ is a critical temperature and $\gamma^o = \gamma$ at $T = 0°K$. The exponent n is determined by experiments and it is near unity for metals and for many organic liquids. It should be noted that the surface heat capacity $C_P^s$ can also be determined in principle from the temperature dependence of $G^s$ since Eq. 7.

$$C_P^s = -T\left(\frac{\partial^2\gamma}{\partial T^2}\right)_P \tag{7}$$

However, the experimental data of $\gamma$ as a function of temperature is far from being accurate enough to allow surface heat capacity determination this way.

### A. Estimation of Specific Surface Free Energies

The specific surface free energy for an unstrained phase is proportional to the change of the total free energy of the system due to changes in the surface area, $dG_P = G^s dA$. Thus, creation of more surface always increases the total free energy of the system. Since atomic bonds must be broken to create surfaces, it is expected that the specific surface free energy be related to the heat of vaporization which is related to the energy input necessary to break all the bonds of atoms in the condensed phase. The heat of vaporization is defined as a molar quantity (energy per gram atom) while the specific surface free energy is defined as energy per unit area. In order to compare the two values we must convert the specific surface free energy to molar surface free energy.[7] Because of differences in the densities of various metals, they will have differing numbers of atoms occupying a unit area. Let us

define an area A as the area occupied by Avogrados number of atoms N. The atomic volume $V_a$ is given by

$$V_a = \frac{V_m}{N} = \frac{M}{N\rho} \tag{8}$$

where $V_m$ is a molar volume, $\rho$ is the density and M the atomic weight. Thus, the area per atom $A_a$ is given by Eq. 9

$$A_a = f(V_a)^{2/3} = f\left(\frac{M}{N\rho}\right)^{2/3} \tag{9}$$

where f is the structure factor that corrects for the assumption that the surface is the (100) face of a simple cubic lattice (this was implicitly assumed in using $V_a^{2/3}$ as a surface area). The value of f is 1.09 for melts of fcc solids, 1.12 for melts of bcc solids and 1.14 for molten bismuth, tin and antimony (orthorombic in the solid state).[8] The molar surface area is biven by Eq. 10 and the molar surface tension or molar surface free energy of the liquid is defined as Eq. 11.

$$A = NA_a = fN^{1/3}\left(\frac{M}{\rho}\right)^{2/3} \tag{10}$$

$$\gamma_{\ell m} = A\,\gamma_e\,(T) \tag{11}$$

Now we can proceed to compare $\gamma_{\ell m}$ directly to the heat of vaporization since both quantities are known from experiments for over 22 liquid metals. The plot of $\gamma_{\ell m}$ at the melting point for each metal versus their heats of vaporization, $\Delta H_{vap}$ is shown in Fig. 1. The least squares fit yields the relationship

$$\gamma_{\ell m} = 0.15\ \Delta H_{vap} \tag{12}$$

All of the experimental data fit this equation with a standard deviation of 8%. Although the $\gamma_{\ell m}$ versus $\Delta H_{vap}$ correlation that is expressed in Eq. 11 appears to hold very well for liquid metals, it does not hold for organic liquids of various types. In Fig. 2, surface tensions of various organic liquids at the melting point are plotted against the heats of vaporization assuming f = 1. As can be seen, the data are widely scattered reflecting the diversity and complex bonding characteristics and packing in these liquids.

For monatomic solids, surface tension determination is more difficult and the available experimental data are scarce and often determined only at one temperature. Nevertheless, all of the collected data are converted to molar surface tensions, $\gamma_{sm}$, and are plotted against the heats of sublimation, $\Delta H_{sub}$, for various metals in Fig. 3. A least squares fit yields a relationship

$$\gamma_{sm} = 0.16\ \Delta H_{sub} \tag{13}$$

There is an excellent agreement between the experimental values and those calculable from Eq. 12, and the standard deviation is 8%. Thus it appears that at least for metals the surface tension may be estimated when direct experimental determination is difficult or lacking. In developing the above correlations the temperature dependence of the surface tensions has been neglected although they are certainly not negligible. Inspection of the $d\gamma/dT$ values reveal that most surface tensions change by no more than 5% in a 100° temperature interval. This variation is not greater than the uncertainty of most surface tension experiments. Thus, the surface tension may be taken as constant in most cases as long as the temperature range of experimental interest is limited.

There are several models proposed in the literature to correlate surface tensions of metals to their heats of vaporization or heats of sublimation. There are also models that correlate surface tensions to the degree of charge redistribution that takes place at a freshly made surface. Schmit and Lucas[9] proposed that the surface free-energies of metals are mainly due to the change in plasmon density caused by the introduction of the new surface. Their computed surface free energies fall within 30% of the measured values.

One of the most successful calculations of the surface free energies of metals was carried out by Lang and Kohn.[10] They calculated the charge densities at surfaces from first principles. In theory, the charge density of the inhomogeneous electron gas at the surface is calculated taking local exchange and correlation energies into account. Both a positive charge model and a pseudopotential potential model of the metal ions are used. The resulting surface energies are in fair agreement with the measured surface tension values for eight simple metals (typical errors are of the order of 25%).

There are several calculations which estimate the surface tensions of ionic metals[11] and noble gas crystals.[12] In these computations, a suitable potential function is used that gives a potential energy of interaction between pairs of atoms as a function of the distance of separation only. Then the total energy for the surface layer is obtained as the sum of the interaction of the pairs. For noble gas crystals, the Lennard-Jones 6-12 potential function has been used. The computations are carried out in parts. First, a surface is produced by breaking bonds, that is, removing atoms adjacent to the newly created surface atoms. During this process, the atoms in the newly created surface are held rigidly in their equilibrium positions which

they would have occupied in the bulk of the solid. Then the surface atoms are allowed to relax into a new equilibrium position by displacement perpendicular to the surface plane. This relaxation process always decreases the total specific surface energy. Since atoms on the surface have fewer neighbors, and the crystal symmetry is lowered with respect to atoms in the bulk, the displacement and subsequent lowering of the specific surface energy can be large. The specific surface energy may be written as

$$E^S = E^S(0) + \Delta E^S \tag{14}$$

where $E^S(0)$ is the specific surface energy of the rigid lattice and $\Delta E^S$ is the relaxation energy. These two terms have opposite signs. These calculations indicate that the magnitude of the specific surface free energies are roughly proportional to the heats of atomization of the various solids. Weakly bonded rare gas crystals have low specific surface energies, 20-60 ergs/cm$^2$. Also, their specific relaxation energies are a very small fraction of the total surface energy. For ionic crystals, the specific surface free energies are about 100-300 ergs/cm$^2$ and the relaxation energies are high, up to roughly 50% of the total energy, due to the polarization of the ions at the freshly created surface. For metals, the measured specific surface free energies are even higher--400-1,000 ergs/cm$^2$--but the relaxation energies are generally small, no more than 2-6% of the total energy.

B. The Effect of Surface Tension on Growth and Surface Reactions

Comparison of the surface tension values listed in Table 1, with the surface tensions of metals (from Fig. 3) indicate that oxides have, in general lower surface tensions. Therefore oxidation of the surface reduces the total free energy of the system in most cases. As a result one may expect the oxide layer to cover the surface as uniformly as possible under conditions near thermodynamic equilibrium. Similarly epitaxial deposition and growth of a metal film on a metallic substrate of higher surface tension should yield a uniform deposit that is spread evenly to cover completely the substrate surface. Very poor spreading of the vaporized film is expected upon deposition of a metal of high surface tension on a low surface tension substrate. In this circumstance the epitaxial growth of the deposit would increase the surface free energy of the system. As a result "island growth" commences, the deposited high surface tension metal will grow as whiskers to expose as much of the low surface tension substrate during the growth as possible.

For example, the lower surface tension silver is expected to spread uniformly over a nickel substrate during epitaxial growth and grow uniformly. In contrast, the higher surface tension nickel would yield a very poor, uneven deposit when grown epitaxially on a silver crystal surface as a consequence of these surface free energy considerations. Of course, the presence of impurities at the surface or difficulties of nucleation may override these surface thermodynamic predictions in some cases.

Condensation of metallic films or nucleation of an oxide at the surface can often be completely stopped by spreading a low surface tension hydrocarbon or fluorinated hydrocarbon compound on the surface. Some of these

compounds reduce the surface tension of metals or oxides so effectively that when the surface is scratched to expose the high surface tension substrate the scratch "heals itself" by spreading of the low surface tension organic compound to cover the exposed metal or oxide surface.

### C. Surface Tension of Multicomponent Systems

The change of the total free energy of a multicomponent system can be expressed with the inclusion of the surface term as[1-3]

$$dG = SdT + VdP + \gamma dA + \sum_i \mu_i dn_i \qquad (15)$$

Here $\mu_i$ is the chemical potential of the ith component and $dn_i$ is the change in the number of moles of the ith component. All other symbols have their usual meanings. At constant temperature and pressure, Eq. 15 can be rewritten as

$$dG_{T,P} = \gamma dA - \sum_i \mu_i dn_i \qquad (16)$$

where the minus sign indicates the decrease of the bulk concentration of the ith component. This equation shows that the surface tension, $\gamma$ is no longer equal to the specific surface free energy per unit area for a multicomponent system. Using simple arguments in which number of moles of the condensed phase are transferred to the freshly created surface, the Gibbs equation can be derived,

$$d\gamma = -S^s dT - \sum_i C_i^s \, d\mu_i \qquad (17)$$

where $C_i^s$ is the surface concentration of the ith component. Just like the free energy relations for bulk phases, the Gibbs equation predicts changes in surface tensions as a function of experimental variables such as temperature and the surface concentration of various components. This equation is

fundamental in determining many surface properties. We shall demonstrate its usefulness through application to determine the surface composition in equilibrium with the bulk composition. As it will be seen, as a result of the Gibbs equations, the surface composition in equilibrium with the bulk for a multicomponent system can be very different from the bulk composition.

D. The Surface Composition of an Ideal Binary Solution

For an ideal binary solution at a constant temperature, the Gibbs equation may be expressed as[1]

$$d\gamma_T = -C_1^s \, d\mu_1 - C_2^s \, d\mu_2 \tag{18}$$

It has been shown[1] that the surface tension of component 1 in an ideal dilute solution is given by

$$\gamma = \gamma_1 + \frac{RT}{a} \ln \frac{X_1^s}{X_1^b} \tag{19}$$

where $\gamma_1$ is the surface tension of the pure component and a is the surface area occupied by 1 mole of component 1. Perfect behavior is assumed, i.e., the surface areas occupied by the molecules in the two different components are the same ($a_1 = a_2 = a$). $X_1^s$ and $X_1^b$ are the atom fractions of component 1 in the surface and in the bulk respectively. It is also assumed that the surface consists only of the topmost atomic layer (monolayer model). For a two component system, Eq. 19 can be rewritten in the form,[2]

$$\frac{X_1^s}{X_2^s} = \frac{X_1^b}{X_2^b} \exp[(\gamma_2-\gamma_1)\frac{a}{RT}] \tag{20}$$

where $X_1^s$ and $X_1^b$, $X_2^s$ and $X_2^b$ have their meaning defined above, and $\gamma_1$ and $\gamma_2$ are the surface tensions of the pure component and the other symbols have their usual meanings. According to Eq. 20, the component that has the smaller

surface tension will accumulate on the surface. The exponential dependence of the surface atom fraction ratio on the surface tension difference ensures that if this model has any validity, the surface composition will always be quite different from the bulk composition. It was shown above that the surface tensions of liquid metals are in the range of 0.5 to 1.5 Newton/meter. Assuming a surface tension difference as small as 0.05 Newton/meter, one obtains, at 1,000°K and a mean surface area of $10^{-19}$ $m^2$/atom, $X_1^s/X_2^s = (X_1^b/X_2^b) \times 1.44$, a considerable surface excess of component 1 which was assumed to have the lower surface tension. There are many surface active organic liquids that demonstrate the accumulation of the component with lower surface tension at the surface. Many alloys that form solid solutions that are nearly ideal, also obey Eq. 20.

Auger Electron Spectroscopy, (AES), provides a means to measure directly the surface composition by experiment.[13] This nondestructive technique detects the Auger electrons emitted from atoms of the condensed phase, liquid or solid. As long as low energy Auger peaks are studied, the Auger electrons detected are emitted primarily by the atoms of the topmost atomic layer. It has been shown that the Auger peak heights are proportional to the concentrations of the corresponding atomic species. Auger spectroscopy thus offers a means to analyze each layer with respect to all its constituents. The surface composition of several alloys has been studied already by Auger electron spectroscopy. These include the nickel-copper[14] and the silver-palladium[15] system as well as the lead-indium system.[16] Perhaps the lead-indium alloy system has been studied in the greatest detail. For a given bulk composition the lead-indium ratio on the surface is found to be about five

times that in the bulk. For the various bulk compositions studied, it is apparent that the surface is always considerably richer in lead than the bulk as predicted by the monolayer model. Perhaps a more sensitive probe of the concentration changes in the surface phase is a measurement of the temperature dependence of the Auger peak intensities. In the bulk phase, the composition remains unchanged as a function of temperature for a given sample. In the surface phase, however, the composition should change as a function of temperature as indicated by Eq. 20. Figure 4 shows the logarithm of the atom fraction ratio of lead to indium against the reciprocal temperature. The $\log X_{Pb}/X_{In}$ vs 1/T plot yields a straight line with a positive slope. According to the theoretical model given in Eq. 20 the slope should be 965 while the experimental data yields a slope of 330. Thus, there is only qualitative agreement between the surface characteristic predicted by the ideal monolayer model and the surface characteristics of the lead-indium system.

The presence of ambient gases that form chemical bonds of various strengths with the consituents of the alloy may change markedly the surface composition. It has been shown by Bouwman and Sachtler[17] that the surface of a gold-platinum alloy becomes enriched in platinum and the surface of a silver-palladium alloy becomes enriched in palladium in the presence of CO. In the absence of CO, in vacuum, the gold-platinum surface has excess gold and the silver-palladium surface has excess silver. The formation of the strong carbonyl bonds with platinum and palladium provides a driving force for the migration of these metal atoms to the surface and changes of the surface composition. Thus, in the presence of adsorbed gases that form chemical bonds with the surface atoms or in the presence of impurities that segregate at the surface the binary surface phase is converted to a ternary system and

should be studied accordingly. It has been noted that the segregation of carbon or sulphur at the surface may have a marked effect on the surface composition of the alloy constituents.

## E. Thermodynamic Properties of Curved Surfaces

In order to minimize the surface area, and thereby to decrease the excess surface free energy, liquids assume a curved surface in equilibrium.[1-2] The radius of curvature will depend on the pressure difference on the two sides of the interface and on the surface tension. Consider a drop of liquid with internal and external pressures $P_{in}$ and $P_{ex}$ respectively and with a surface tension $\gamma$. In equilibrium the radius of curvature, r of the droplet is related to these quantities as

$$(P_{in}-P_{ex}) = \frac{2\gamma}{r} \tag{21}$$

This equation helps to explain many of the properties of liquid surfaces. First of all, it indicates that in equilibrium a pressure difference can be maintained across a curved surface. The smaller the droplet or the larger the surface tension, the larger the pressure difference. For a flat surface, on the other hand, $r \to \infty$, and the pressure difference normal to the interface vanishes. Let us now consider how the vapor pressure of a droplet depends on its radius of curvature r. This is expressed by the well-known Kelvin equation

$$\ln\left(\frac{P}{P_o}\right) = \frac{2\gamma V_m}{RTr} \tag{22}$$

$P_o$ is the vapor pressure over a flat surface where $1/r$ is equal to 0, and $V_m$ is the molar volume. We see that, according to Eq. 22, small particles have higher vapor pressures than larger ones. If we substitute instead of

the vapor pressures, solubilities, which for ideal solutions are proportional to vapor pressures, we find that small particles of solids have greater solubilities than large particles. If we have a distribution of particles of different sizes, a common occurrence in powder metallurgy and for many thin films, we will find that the larger particles will grow at the expense of the smaller ones, as predicted by Eq. 22. This is the cause of sintering of small particles as they are being heated to elevated temperatures but well below the melting point. We find, from inspection of Eq. 22, that grain growth can be induced not only by increasing the temperature of the small particles, but also by increasing the surface tension. On the other hand, sintering or grain growth can be diminished or stopped by decreasing the surface tension, for example by adsorbing a gas such as oxygen or carbon monoxide. Oxides, in general, have lower surface tensions than do metal particles. It should be noted that such differences in vapor pressure or solubility that depend on particle size can only be observed for particles smaller than 100Å. Above this value, for the usual values of the surface tension ($P/P_o$) approaches unity rapidly.

Let us turn our attention to the interfacial tension, that is, the surface tension that exists at the interface of two condensed phases. Let us place a liquid droplet on a solid surface. The droplet either retains its shape and forms a curved surface or it is spread evenly over the solid. These two conditions indicate the lack of wetting or wetting of the solid by the liquid phase, respectively. The contact angle between the solid and the liquid, to a large extent, permits us to determine the interfacial tension between the solid and the liquid.[18] The contact angle is defined by

Fig. 5. If the contact angle is large, ($\theta$ is approaching 90°) the liquid does not readily wet the solid surface. If $\theta$ approaches 0, complete wetting of the solid surface takes place. For $\theta$ larger than 90°, the liquid tends to form sphere-shaped droplets on the solid surface that may easily run off; i.e., the liquid does not wet the solid surface at all. Remembering that the surface tension always exerts a pressure tangentially along a surface, the surface free energy balance between the surface forces acting in opposite directions at the point where the three phases, solid, liquid and gas meet, is given by

$$\cos\theta = \frac{\gamma_{sg} - \gamma_{s\ell}}{\gamma_{\ell g}} \tag{23}$$

Here, $\gamma_{\ell g}$ is the interfacial tension at the liquid-gas interface, $\gamma_{sg}$ and $\gamma_{s\ell}$ are the interfacial tensions between the solid-gas and the solid-liquid interfaces, respectively. Thus, knowing $\gamma_{\ell g}$ and the contact angle in equilibrium at the solid-liquid-gas interface, we can determine the difference $\gamma_{sg} - \gamma_{s\ell}$, but not their absolute values.

The usefulness of a lubricant is determined by to what extent it wets the solid surface and maintains complete coverage of the surface under various conditions of use. The strength of an adhesive is determined by the extent it lowers the surface free energy by adsorption on the surface. The work of adhesion is defined as

$$W_A^s = \gamma_{\ell,0} + \gamma_{s,0} - \gamma_{s\ell} \tag{24}$$

where $\gamma_{\ell,0}$ and $\gamma_{s,0}$ are the surface tensions in vacuum of the liquid and solid, respectively. In general, solids and liquids that have large surface tensions form strong adhesive bonds, i.e., have large works of adhesion.

The work of adhesion is in the range of 40-150 ergs/cm$^2$ for solid-liquid pairs of various types. Organic polymers often make excellent adhesives because of the large surface areas covered by each large organic molecule. The adhesive energy per mole is much larger than that for adhesion between two metal surfaces or between a liquid and a solid metal because of the many chemical bonds that may be formed between the substrate and the adsorbed organic molecule.

If one plots the surface tensions of various organic liquids against their contact angles on a given solid surface a linear relationship is obtained. One such plot is shown in Fig. 6 for polyethylene, where the various data points correspond to different liquids.[18] Thus, the contact angle determination can be used to estimate surface tensions of liquids in addition to wettability. Knowledge of the contact angle between the solid and the liquid can also be used to estimate the surface tension of solids according to the methods suggested by Good .[19]

Recently, Ferrante and Smith[20] have calculated the adhesive binding energies at the Zn, Mg and Al metal-metal interfaces by taking into account the electron-ion, ion-ion and electron-electron interactions separately. The binding energies were in order of decreasing strength Al-Al > Al-Zn > Al-Mg > An-Mg > Mg-Mg. This trend is substantiated by experiments. The binding energy was calculated as a function of the distance of separation as well. The electron exchange energy was found to be an important part of the adhesive binding energy.

## III. THE STRUCTURE OF SURFACES

Figure 7 shows the surface of polycrystalline copper under 200× magnification. The surface exhibits many irregularities. There are crystallites which are separated by boundaries which give them the appearance of small islands of roughly equal size. Figure 8 is an electron microscope picture of the same surface using a magnification of 5,000×. The surface exhibits pits at this magnification with walls that appear to be terraced. There are flat areas between the terraces separated by ledges many atomic layers in height. In an optical microscope or on the scale of a scanning electron microscope, the surface appears to be heterogeneous. Many surface sites are distinguishable. There are grain boundaries between small crystallites and atomic terraces and ledges in which the atoms must be surrounded by different numbers of neighbors.

Let us now view the surface on an atomic scale. Both low energy electron diffraction (LEED) and field ion microscopy (FIM) are techniques that give us information about the atomic structure of surfaces. These techniques will be discussed in a subsequent chapter. Briefly, in low energy electron diffraction, electrons in the energy range of 20-150 eV are allowed to backscatter from one face of the crystal. The elastically scattered fraction can undergo diffraction from ordered domains of surface atoms and can provide information about the surface structure. In Fig. 9, a typical diffraction pattern obtained from the (111) face of platinum at various beam voltages is displayed. The sharp diffraction spots clearly indicate that the surface is ordered on an atomic scale. The technique of field ion microscopy will also be discussed in a subsequent chapter. Briefly, under the influence of a large electric field of about $10^9$ volts/cm at a small crystal tip, He atoms are

ionized. The positive ions are repelled from the surface radially and accelerated onto a fluorescent screen. The intensity of any part of the screen is proportional to the number of incident He ions. Since the concentration of He ions at each crystal surface depends on the unique atomic and charge densities in the different planes, the various crystal surfaces of the tip end can be identified by studying the intensity contrast of the fluorescent screen. The various crystal faces can be readily distinguished and identified as indicated by Fig. 10 which exhibits a typical field ion microscope picture of a tungsten tip surface.

The techniques of low energy diffraction and field ion microscopy, indicate that the surface appears to be ordered on an atomic scale. Most of the surface atoms occupy equilibrium atomic positions that are located in well-defined rows separated by equal interatomic distances. This atomic order is predominant in spite of the fact that there are large numbers of atomic positions on the surface where atoms have different numbers of neighbors. The model that describes the surface topology of a monatomic crystal on an atomic scale is shown in Fig. 11. The surface may have atoms in the various positions depicted by this figure. There are atoms in the surface at kink positions and in ledge positions, and there are adatoms that are adsorbed on the surface.[2] Atomic movement from one position to another occurs by surface diffusion. To the first approximation, the binding energy of the surface atoms is proportional to the number of nearest and next-nearest neighbors. Thus, atoms at a ledge are bound more strongly than are adatoms, for example. In equilibrium, there is a certain concentration of all of these surface species with those species predominating whose binding energies are greatest. Thus, the adatom concentration on fairly well-equilibrated surfaces should be very small indeed.

# IV. THE ATOMIC STRUCTURE OF CLEAN SURFACES

## A. Nomenclature

Most of our information about the atomic surface structure has come from low-energy electron diffraction studies.[21] The nature of low-energy electron scattering from surfaces and the low-energy electron diffraction experiment will be discussed in the next chapter. Here, we shall concentrate on the experimental findings and their interpretations. First, however, we shall have to introduce the nomenclature that is currently used to identify the various diffraction spots in the pattern and the surface structure that corresponds to it. Figure 9 showed the diffraction pattern obtained from the (111) crystal face of platinum at four different electron energies. At low energies, only first-order diffraction beams are detectable. The six-fold rotational symmetry reflects the rotational symmetry of the atomic surface structure that is responsible for the diffraction. As the electron energy is increased, the wavelength of the incident electrons decreased [$\lambda(\text{Å}) = \sqrt{150/\text{eV}}$] and the higher order diffraction beams also become visible appearing at the edge of the diffraction pattern.

The various diffraction beams are identified by their two-dimensional Miller indices that are shown in Fig. 12. The diffraction pattern in Fig. 12 was taken at normal electron beam incidence ($\theta = 0$) so that the (00) or specular beam cannot be seen. In Fig. 12, the azimuthal angle that indicates the degree of rotation of the crystal plane about the surface normal is also shown. The two-dimensional Miller indices used to identify the diffraction beams in the (110) crystal face of a face-centered cubic solid that exhibit twofold rotational symmetry, is shown in Fig. 13. The Miller Index notation is the commonly accepted way to identify the various diffraction beams. The

diffraction beams that are identified this way are predicted from crystal surfaces in which the atoms occupy positions expected from the projection of the bulk unit cell to the surface. The real space surface structure that gives rise to the diffraction patterns of Fig. 9 is called briefly a (1×1) surface structure. The shorthand notation that is used in describing such a "normal" structure is Pt(111)-(1×1). Of course, this notation describes the rotational symmetry and the size of the surface unit mesh only. If there is an expansion or contraction of the first layer of atoms with respect to the second layer below the surface in the z direction, (i.e. normal to the surface). This notation will not identify this change as long as the relative atomic positions in the surface layers remain unchanged.

There are several crystal faces where the surface atoms are arranged in such a way that the surface unit mesh is different from that expected from the projection of the bulk unit cell. One such case is the (111) face of silicon. Figure 14b shows a diffraction pattern expected from a (1×1) silicon surface structure. On heating this surface to above 375°C, the surface reconstructs, and the diffraction pattern shown in Fig. 14a results. There are diffraction beams in positions that can be identified by fractional Miller indices such as (1/7) 1, (2/7) 1, ···, (6/7) 1, between the (00) and (11) diffraction beams, for example. Such a diffraction pattern indicates the appearance of a new surface structure with unit cell that is parallel to the unit cell of the (1×1) surface structure but seven times as large. Thus, the surface structure is denoted by our abbreviated notation as Si(111)-(7×7). Sometimes, the identification of the surface structure is not so easy. If

the unit cell of the reconstructed surface is rotated with respect to the (1×1) unit mesh and of different size, a complex diffraction pattern may result. A more unambiguous way of identifying the diffraction pattern that allows the determination of the unit cell of the real lattice as well is via the reciprocal lattice matrix. To see how this works, let us consider a (2×2) surface structure that is characterized by a diffraction pattern with diffraction beams in the 1/2 order positions. The diffraction pattern or reciprocal lattice space net may be regarded as being generated from the basis vectors $\bar{a} = 0\cdot\bar{x} + \frac{1}{2}\bar{y}$ and $\bar{b} = \frac{1}{2}x + 0\cdot y$ where the first order diffraction spots from the clean surface would have the indices (10) and (01). The primitive translation vectors of the surface net are given in terms of the translation vectors of the substrate. The resulting reciprocal lattice matrix is $\underset{\approx}{G} = \begin{vmatrix} 0 & 1/2 \\ 1/2 & 0 \end{vmatrix}$. Now the real space lattice matrix, is given by $\underset{\approx}{A} = \begin{vmatrix} 0 & 2 \\ 2 & 0 \end{vmatrix}$. In general if $\underset{\approx}{G}$ is given by $\underset{\approx}{G} = \begin{vmatrix} a_{11} & a_{12} \\ a_{21} & a_{22} \end{vmatrix}$ then

$\underset{\approx}{A} = \frac{1}{|G|} \begin{vmatrix} a_{22} & -a_{12} \\ -a_{21} & a_{11} \end{vmatrix}$. Thus, we can readily generate the real space lattice vectors from the reciprocal space lattice vectors using the reciprocal lattice matrix and inverting to the real space lattice matrix.

Recently, the surface structure of a great variety of crystal faces that have high Miller indices have been studied. For example, a (755) three-dimensional Miller index is obtained by cutting from a (111) crystal face of a fcc solid at 9.5° in the direction of the (100) face.[22] Analysis of the diffraction features, to be discussed below, indicates that such a high Miller Index surface has a stepped atomic surface structure.[23] This surface

structure is characterized by atomic terraces of, on an average, six atoms wide and (111) orientation separated by steps of one atom in height of (100) orientation. Such an ordered step array can be completely designated by the width and the orientation of the terraces, and the height and orientation of the steps. The stepped surface with the characteristics described above can be represented by the notation Pt(S)-[6(111)×(100)], where the postscript S indicates a stepped platinum surface, 6 indicates the width of the terrace in numbers of atomic rows, (111) indicates the orientation of the atoms in the atomic rows of the terrace, and the (100) indicates a step of (100) orientation and 1 atom in height. In general, the notation M(S)-[m(111)×n(100)] designates the stepped surface. In the case of steps of monatomic height, the prefix n = 1 may be omitted.

B. Unreconstructed Surfaces that Exhibit Contraction (Expansion) Perpendicular to the Surface Plane or Changes in Chemical Composition

The intensities of low-energy diffraction beams as a function of incident electron energy and angle of scattering has been determined for several materials, mostly monatomic metals. These intensities were measured for the (111), (100), and (110) crystal faces of aluminum,[24] the (100) and (111) crystal faces of nickel,[25] the (100) and (111) faces of copper,[26] (111) crystal face of silver,[27] and the (100) crystal face of lithium fluoride.[28] Using these experimental intensity data, calculations have been performed to determine the position of surface atoms based on the theory in which the only adjustable parameters are the atomic positions at the surface. Diffraction beam intensity data is available for several other monatomic and diatomic solids, but for these structure analysis has been lacking. The theory used to calculate the

intensities and the details of these calculations are reviewed by several papers.[29-32] The calculations indicate that the upper layer spacing in the same as predicted from the bulk x-ray unit cell to within 5% of the interatomic distance for atoms in the aluminum (100) and (111) and copper (100) and (111) crystal faces, as well as for nickel in the (111) and (100) crystal faces. These calculations can determine the atomic position in the surface layer to within 0.1 Å. However, the (110) face of aluminum was found to be contracted by about 10-15% from the bulk interlayer spacing. The best agreement between calculations and experimental intensities are obtained when the surface atoms are allowed to move closer to the second layer. Figure 15 shows the calculated and experimental intensities from the (100) aluminum surface. It can be seen that the agreement between calculated and experimental intensities is quite adequate to draw conclusions as to the interlayer spacing between the first and second layers. Figure 16 shows the calculated and experimental intensities for the aluminum (110) crystal face.[33] One can see that the intensity data is very sensitive to the interlayer spacing. Laramore and Switendick[34] found that for the (100) face of lithium fluoride, the top lithium and fluoride ion sublayers were separated by about 0.25 Å. The lithium ion sublayer appears to be contracted by a greater amount towards the bulk.

It should be noted that all these crystal faces exhibit diffraction patterns that are characteristic of unreconstructed surfaces. That is, the atoms lie in the surface in positions that are expected from their bulk unit bell. Nevertheless, there is atomic relaxation in the z direction, perpendicular to the surface. It appears that the more open surfaces show a tendency toward relaxation, either contraction or expansion, in the z direction.

Chemical surface studies frequently compliment structural studies by low energy electron diffraction. Excellent examples of this are the LEED-Auger studies of alkali halide surfaces by Gallon et al.[35], and studies of the surface structure of lithium hydride by Holcomb, et al.[36] These researchers have found that the composition of the surface is different from that of the bulk composition. There is evidence of precipitation of the alkali metal on the alkali-halide surface and/or evolution of halogen. In the case of lithium hydride, there is evidence of build-up of lithium metal near the lithium hydride surface. During these changes in the chemical composition at the surface the diffraction pattern remained characteristic for a (1×1) unreconstructed surface structure. Thus, it appears that in addition to lowering the surface free energy by changing the interatomic distances at the surface, the surface free energy may be lowered by changing the stoichiometry at the surface. The introduction of excess defects, positive or negative ion vacancies, appear to bring about a surface structure that is more stable than the one with chemical composition similar to that in the bulk. Although similar surface chemical studies have not been carried out on many other materials, it is expected that compound semiconductors (those formed from elements in the II-VI and III-V groups in the periodic table) may also show similar effects. It is hoped that nonstoichiometry in the surface layer will be studied and correlated with surface crystallography data obtained by measuring diffraction beam intensities and with model calculations used to determine the atomic positions at the surface.

## C. Surface Reconstruction

We define surface reconstruction as a state of the clean surface when its LEED pattern indicates the appearance of a surface unit mesh that is different from the usual bulk-like (1×1) unit mesh. Low energy electron diffraction studies have indicated that most low Miller index metal surfaces that have been studied so far have surface structures that are expected from the projection of their bulk x-ray unit cells. There may be changes in the interlayer distances between the first and second layer but contraction or expansion in the z direction can take place without changing the (1×1) surface unit cell size or orientation. For alkali halides there is enhanced non-stoichiometry in the surface layer,[35] but this change in chemical composition does not seem to change the observed surface unit mesh. However, there are several metal surfaces where the surface structure is very different from that predicted by the bulk unit cell, and semiconductor surfaces more frequently than not exhibit surface reconstruction. Let us first discuss reconstructed semiconductor surfaces. One of the best studied examples is that of the Si(111) surface.[37] Upon cleaving, at 25°C, the surface exhibits a (2×1) surface structure. On heating to about 370-400°C, the surface structure changes. According to Mönch, the (2×1) structure converts to the (7×7) surface structure which is shown in Fig. 1. The (7×7) structure is then the stable surface structure of the (111) crystal face. Joyce,[38] however, reported that in the presence of trace impurities such as iron or nickel, the (2×1) surface is converted first to a (1×1) structure at 400°C, and the (7×7) structure forms only upon heating to 700°C. There is enough evidence to indicate that the temperature at which the impurity-stabilized (1×1) surface structure transforms

into the (7×7) structure depends markedly on the amount and nature of trace impurities on the surface. Other crystal faces of silicon, the various crystal faces of germanium, gallium arsenide, and other III-V semiconductor compounds were also found to undergo reconstruction. Table 2 lists the surface structures of reconstructed surfaces of semiconductors that have been uncovered so far.

There are several theories of reconstruction. Taloni and Hanneman.[39] showed that relaxation of surface atoms out of the surface plane increases the overlap of localized electron orbitals, thereby lowering the surface free energy. Trullinger and Cunningham[40] proposed that the softening of phonon modes at the surface gives rise to the periodic relaxation of surface atoms. All of these models indicate that surface reconstruction is indeed possible and results in the lowering of surface free energy, but they do not predict the unique surface structure that is likely to be most stable. Since transformations from one surface structure to another can take place on both silicon and germanium surfaces as a function of temperature, the magnitude of the surface energies associated with the two structures are within $\sim kT$ of each other. Such a small energy difference should make it difficult to predict their relative stability.

Among metals, the most consistent change in surface structure was observed for the (100) crystal faces of three, 5d transition metals that are neighbors on the periodic table, gold, platinum and iridium. All three exhibit the so-called (5×1) or (5×20) surface structure that is shown in Fig. 17. There are two perpendicular domains of this surface structure, and there are 1/5, 2/5, 3/5, and 4/5 order spots between the (00) and (10)

diffraction beams. The surface structure is not quite as simple as the shorthand notation indicates as is shown by the splitting of the fractional order beams. The surface structure appears to be stable at all temperatures from 25°C to the melting point, although its study at the elevated temperatures can bring impurities from the bulk to the surface that can cause a transformation of this structure to the impurity stabilized (1×1) surface structure.[41] Carbon at the surface that may diffuse out of the bulk in minute quantities or adsorbed gases of various types (CO, $C_2H_2$, etc.) can cause the surface atoms to relax back to their bulk-like (1×1) atomic positions.[41] The diffraction beam intensities of the (5×20) structure are under close investigation in many laboratories. Preliminary calculations favor a model in which the surface atoms assume a distorted, hexagonal configuration by out-of-plane buckling. The apparent (5×20) unit cell is the result of coincidence of the atomic positions of atoms in the surface with atoms of the undistorted second layer below. Table 2 also lists the reconstructed surfaces of various metals that were found so far.

Surface atoms in any crystal face are in an anisotropic environment which is very different from that about bulk atoms. The crystal symmetry that is experienced by each bulk atom is markedly lowered when the atom is placed on a surface. The change of symmetry and the lack of neighbors in the direction perpendicular to the surface permits displacement of surface atoms in ways that are not allowed in the bulk. Surface relaxation can give rise to a multitude of surface structures depending on the electronic structure of a given substance. It is indeed surprising that there are so many solid surfaces that do not exhibit surface reconstruction. Upon adsorption of

gases such as oxygen or hydrogen, or in the presence of impurities, surface reconstruction may be induced or inhibited, as indicated by many recent experiments.

Changes of chemical composition at the surface can produce marked changes in surface structure. $\alpha$-$Al_2O_3$ and $V_2O_5$ develop new surface structures upon the loss of oxygen from the crystal lattice by heat treatment in vacuum at elevated temperatures.[2] The new surface structure appears to be characteristic of the reduced, oxygen deficient surface. For $\alpha$-alumina this transformation is reversible; heating in oxygen at $> 10^{-4}$ Torr regenerates the (1×1) surface structure.

## D. Stepped High Miller Index Surfaces

In recent years there have been several low energy diffraction studies on crystals cut to expose high Miller Index planes. Such studies have been carried out on platinum,[22] copper,[42] germanium,[23] gallium arsenide[23] and uranium dioxide single crystals.[43] Perhaps the most detailed studies of high Miller Index surfaces have been carried out on platinum.[44] Figure 18 shows one crystallographic zone of platinum and the points indicate the direction of the cuts that were made. The back-reflection Laue x-ray pattern of one of the surfaces clearly indicates that it was cut 6.5° from the Pt(111) crystal face. This surface has a Miller Index (997). The low energy electron diffraction pattern that is obtained from this surface is shown in Fig. 19. The rotational symmetry of the diffraction pattern clearly indicates that ordered domains with (111) orientation predominate on this surface. The patterns differ from those expected from crystals with low index faces only in that the diffraction beams are split into doublets or triplets at certain voltages.

It has been shown[23] that this splitting is a function of ordered steps existing on the surface. The diffraction features are as sharp as those observed with a nominally flat, low index surface. At a given beam voltage, the doublet separation is dependent on the distance between the steps, i.e. the terrace width. Kinematic analysis[23] shows that the electron energies at which the doublets exhibit maximum intensity depend on the step height. For the (00) diffraction beam, the voltages at which doublet spots of equal intensity exists are given by

$$V_{00}(\text{doublet max}) = \frac{150}{4d^2}(S^2) \qquad (25)$$

where d is the step height and S is an integer with half-integral values. Since the electron energy at which the doublets have equal intensity, is inversely proportional to $d^2$, the voltage-dependence of the intensity is a sensitive measure of step height which can then readily be determined. From the doublet separation, the terrace width can be calculated. This analysis indicates that this particular surface has (111) orientation terraces of 9 atoms in width. Since it was cut in the (110) direction, it must have (111) orientation steps of 1 atom in height. Thus, the notation Pt(S)-[9(111)×(111)] is appropriate to identify this crystal face. Figures 20, 21 and 22 identify the diffraction patterns and the schematic representation of the atomic structures of several stepped surfaces that were cut in different directions, as indicated in Fig. 18, in that particular crystallographic zone. All of these crystal faces that were studied (with the exception of the Pt(S)-[4(111)×(100)] crystal face) exhibit remarkable thermal stability. These surfaces can be heated in vacuum to at least 1100°C without appreciable deterioration of the surface structure. The stepped surface structures are

obtained after ion bombardment and subsequent annealing of an initially disordered surface. After chemisorption of various hydrocarbons or oxygen and hydrogen, the surface structure characteristic of the clean stepped substrate could be readily regenerated. Thus, these ordered steps, which have been noted on other metals and semiconductors as well, must be a general property of high Miller Index surfaces of all types of crystalline materials.

The Pt(S)-[4(111)×(100)] crystal face was not stable when heated in vacuum above 1000°C when faceting produced a new crystal plane with an angle between the newly formed plane and the (111) face estimated to be 31°. The Pt(S)-[4(111)×(100)] could be regenerated under certain conditions of oxygen heat treatment between 800-900°C and subsequent heating in vacuum at 700°C to remove the oxygen. Faceting in general, if it takes place at all, takes place faster in the presence of various hydrocarbons or other adsorbed gases. It appears that the stability of these surfaces is dependent on their step density, and if their step density is too high (or the terrace width is too small), the stability can be markedly reduced. The chemisorption characteristics of these stepped surfaces are entirely different from those of low Miller Index surfaces.[45] In addition, their reactivity in catalytic surface reactions is different, being much more reactive than low Miller Index surfaces.[46] These properties coupled with the remarkable thermal stability of the stepped surfaces make their study both interesting and important in their own right. The variation of surface free energy with orientation is generally described by the γ-plot in which the surface free energy is plotted as a function of crystallographic direction. Herring[47] has shown that at 0°K, the γ-plot has several cusps, that is, local minima, for each plane

of rational Miller Index, and he has demonstrated that as the temperature increases most of the cusps disappear. At higher temperatures, for example 700°K, only those directions corresponding to low index planes will possess cusps. If the presence of stepped surfaces indicate thermodynamic stability in crystallographic directions corresponding to high Miller indices, the $\gamma$-plots should have several minima between the low Miller Index orientations corresponding to the stepped surfaces of various terrace widths. However, the remarkable thermal stability of these stepped surfaces does not necessarily indicate a thermodynamic stability but may be due to the difficult routes the crystal must take to develop an equilibrium shape. The pertinent mechanisms of transport to develop an equilibrium shape are surface diffusion, evaporation and bulk diffusion. The thermodynamic properties of "vicinal" surfaces, a name that has been used to describe stepped surfaces, have been discussed in detail by Burton, Cabrera and Frank.[48] McLean and Mykura[49] have examined the stability of platinum foils of various orientations toward thermal faceting, and the effect of surface diffusion has been treated from an atomic transport point of view by Schwoebel. All of the calculations and the experimental data accumulated indicate that there is no energetically feasible route that is likely to exist by which an array of ordered steps may rearrange to a thermodynamically more favorable surface structure. Thus, the thermal stability of these surfaces is likely to be assured below the melting point. One of the interesting stepped surfaces is the Pt(S)-[7(111)×(310)] face that is shown in Fig. 22. This crystal face exhibits a very large concentration of kinks in each step.[44] In spite of the high kink density, this surface was found to be just as stable as the other stepped surfaces with much lower kink concentrations.

ACKNOWLEDGEMENT

This work was done under the auspices of the U. S. Atomic Energy Commission.

## REFERENCES


1. R. Defay and I. Prigogine, Surface Tension and Adsorption (John Wiley & Sons, Inc., New York, 1966).
2. G. A. Somorjai, Principles of Surface Chemistry (Prentice Hall, New York, 1972).
3. G. N. Lewis and M. Randall, Thermodynamics, revised by K. S. Pitzer and L. Brewer (McGraw-Hill Book Company, New York, 1961).
4. A. W. Adamson, Physical Chemistry of Surfaces (John Wiley & Sons, Inc. (Interscience Division), New York, 1967).
5. W. D. Harkins, The Physical Chemistry of Surface Films (Van Nostrand Reinhold Company, New York, 1952).
6. P. A. Bertrand and G. A. Somorjai, Lawrence Berkeley Laboratory Report LBL 1466, February 1973.
7. A. S. Skapski, J. Chem. Phys. 16, 389 (1948).
8. D. McLachan, Acta Met. 5, 111 (1957).
9. J. Schmit and A. A. Lucas, Solid State Comm. 11, 415 (1972).
   J. Schmit and A. A. Lucas, Solid State Comm. 11, 419 (1972).
10. N. D. Lang and W. Kohn, Phys. Rev. B1, 4555 (1970).
11. G. C. Benson, J. Chem. Phys. 35, 2113 (1961).
12. B. J. Alder, J. R. Vaisnys and G. Jura, J. Phys. Chem. Solids 11, 182 (1959).
13. G. A. Somorjai and F. J. Szalkowski, Advan. High Temp. Chem. 4, 137 (1971).
14. M. L. Tarng and G. K. Wehner, J. Appl. Phys. 42, 2449 (1971).
15. K. Christmann and G. Ertl, Surface Sci.
16. S. Berglund and G. A. Somorjai, J. Chem. Phys., to be published (1973).
17. R. Bouwman and W. M. H. Sachtler, J. Catalysis 19, 127 (1970).
18. W. A. Zisman in Contact Angle, ACS Publication No. 43 (1963).
19. R. J. Good in Contact Angle, ACS Publication No. 43 (1963)

20. J. Ferrante and J. R. Smith, Surface Sci. 32, 11 (1973).

21. G. A. Somorjai and H. H. Farrell, Advan. Chem. Phys. 20, 215 (1970).

22. B. Lang, R. W. Joyner, and G. A. Somorjai, Surface Sci. 30, 440 (1972).

23. M. Henzler, Surface Sci. 19, 159 (1970).

24. F. Jona, IBM J. Res. Dev. 14, 4 (1970).

25. M. G. Lagally, T. C. Ngoc and M. B. Webb, J. Vac. Sci. Tech. 9, 645 (1972).
T. E. Demuth, S. Y. Tong and T. N Rhodin, J. Vac. Sci. Tech. 9, 639 (1972).

26. S. Andersson, Sur. Sci. 18, 325 (1969);
R. J. Reid, Surf. Sci. 29, 603 (1972).

27. M. G. Lagally, Zeit. Naturforschung 25, 1567 (1970).

28. E. G. McRae and G. W. Caldwell, Surf. Sci. 2, 509 (1967).

29. C. B. Duke and C. W. Tucker, Surf. Sci. 15, 231 (1969).

30. S. Y. Tong and T. N. Rhodin, Phys. Rev. Letters 28, 553 (1972).

31. D. W. Jepsen, P. M. Marcus and F. Jona, Phys. Rev. B5, 3933 (1972).

32. J. B. Pendry, J. Phys. C2, 2273 (1963); 2, 2283 (1969).

33. M. R. Martin and G. A. Somorjai, Phys. Rev. B1, 3601 (1973).

34. G. E. Laramore and A. C. Switendick, Phys. Rev. B, to be published.

35. T. E. Gallon, I. G. Higginbothom, M. Prutton and H. Tokutaka, Surf. Sci. 21, 224 (1970).

36. C. E. Holcombe, Jr., G. L. Powell and R. E. Clausing, Surf. Sci. 30, 561 (1972).

37. W. Mönch, Adv. in Solid State Physics 13, 241 (1973).

38. B. A. Joyce, Surf. Sci. 35, 1 (1973).

39. A. Taloni and D. Haneman Surf. Sci. 10, 215 (1968).

40. S. E. Trullinger and S. L. Cummingham, Phys. Rev. Lett. 30, 913 (1973).

41. A. E. Morgan and G. A. Somorjai, J. Chem. Phys. 51, 3309 (1963).

42. J. Perdereau and G. E. Rhead, Surf. Sci. 24, 555 (1971).

43. W. P. Ellis and R. L. Schwoebel, Surf. Sci. 11, 2 (1968).

44. K. Baron, D. Blakely and G. A. Somorjai, Surf. Sci., to be published, 1973.

45. B. Lang, R. W. Joyner and G. A. Somorjai, Surf. Sci. 30, 454 (1972).

46. B. Lang, R. W. Joyner and G. A. Somorjai, J. Catalysis 27, 405 (1972).

47. C. Herring in Structure and Properties of Solid Surfaces, (Univ. of Chicago Press, 1953).

48. W. K. Burton, N. Cabrera and F. C. Frank, Phil. Trans. Royl. Soc. London A243, 299 (1951).

49. M. McLean and H. Mykura, Surf. Sci. 5, 466 (1966).

## Table Captions

Table 1. Selected values of surface tensions of non-metallic solids and liquids and critical surface tensions[18] of polymeric solids.

Table 2. Surface structures of several reconstructed solid surfaces.

Table 1.

| Material | $\gamma\left(\frac{ergs}{cm^2}\right)$ | T(°C) |
|---|---|---|
| He (liquid) | 0.308 | -270.5 |
| $N_2$ (liquid) | 9.71 | -195 |
| Ethanol (liquid) | 22.75 | 20 |
| Water | 72.75 | 20 |
| Benzene | 28.88 | 20 |
| n-Octane | 21.80 | 20 |
| Carbon Tetrachloride | 26.95 | 20 |
| Bromine | 41.5 | 20 |
| NaCl (solid) | 227 | 25 |
| KCl (solid) | 110 | 25 |
| $CaF_2$ (solid) | 450 | -195 |
| MgO (solid) | 1200 | 25 |
| $SiO_2$ (solid) | 307 | 1300 |
| $Al_2O_3$ (solid) | 690 | 2323 |
| Polytetrafluoroethylene | 18.5 | 20 |
| Polyethylene | 31 | 20 |
| Polystyrene | 33 | 20 |
| Poly(vinyl alcohol) | 37 | 20 |
| Poly(methyl methacrylate) | 39 | 20 |
| Poly(vinyl chloride) | 39 | 20 |
| Poly(ethylene terephthalate) | 43 | 20 |
| Poly(hexamethylene adipamide) | 46 | 20 |

Table 2.

| Material | Sixfold Rotation Axis | Fourfold Rotation Axis | Twofold Rotation Axis |
|---|---|---|---|
| Si | (111)-(7×7), (111)-(2×1) | (100)-(2×2), (100)-(4×4) | (110)-(5×2) |
| Ge | (111)-(2×8), (111)-(2×1) | (100)-(2×2), (100)-(4×4) | (110)-(2×1) |
| C(diamond) | (111)-(2×2) | (100)-(2×1) | |
| Te | (0001)-(2×1) | | |
| GaAs | (111)-(2×2), $(\bar{1}\bar{1}\bar{1})$-(3×3) | | |
| GaSb | (111)-(2×2), $(\bar{1}\bar{1}\bar{1})$-(3×3) | | |
| InSb | (111)-(2×2) | (100)-(2×1) | |
| CdS | (0001)-(2×2) | | |
| Pt | | (100)-(5×1) | |
| Au | | (100)-(5×1) | (110)-(2×1) |
| Ir | | (100)-(5×1) | |
| Pd | | (100)-(1×1) | |
| Bi | | | $(1\bar{1}20)$-(2×10) |
| Sb | | | $(1\bar{1}20)$-(6×3) |

## FIGURE CAPTIONS

Fig. 1. Plot of the molar surface tension as a function of the heats of vaporization for liquid metals.

Fig. 2. Plot of the surface tension as a function of the heats of vaporization for organic liquids.

Fig. 3. Plot of the molar surface tension as a function of the heats of sublimation for metallic solids.

Fig. 4. Logarithm of the Pb/In atom fraction ratio as a function of the reciprocal temperature for a sample containing 22.4 atom % lead in the bulk.

Fig. 5. Definition of the contact angle between a liquid and solid and the balance of surface forces at the contact point between the three phases (solid, vapor and liquid).

Fig. 6. The contact angle of various organic liquids on polyethylene as a function of their surface tension.

Fig. 7. Optical microscope picture polycrystalline copper surface at 64× magnification.

Fig. 8. Scanning electron microscope picture of polycrystalline copper surface at 2000× magnification.

Fig. 9. Diffraction pattern of the (111) face of platinum crystal at four different incident electron beam energies a) 51 volts, b) 63.5 volts, c) 160 volts, and d) 181 volts.

Fig. 10. Field Ion Microscope picture of a tungsten tip surface.

Fig. 11. Model of a solid surface on an atomic scale.

Fig. 12. Schematic representation of a diffraction pattern from a (111) face of a face centered cubic solid. The various diffraction beams are identified by two dimensional Miller indices.

Fig. 13. Diffraction beams from the (110) crystal faces of a face centered cubic solid are identified by two-dimensional Miller indices.

Fig. 14. Diffraction pattern from the (111) crystal face of silicon that exhibits a) 7×7) surface structure and b) (1×1) surface structure.

Fig. 15. Experimental and calculated intensity vs electron energy curves for the Al(100) crystal face.

Fig. 16. The experimental I-vs-eV curve (c) is compared to calculated curves for the (00) beam of the aluminum (110) surface. The solid curves (a, b, d) and the dotted curve (d) utilize five phase shifts and four layers in the computation. The dashed curves utilize four phase shifts and four layers. Curve (a) is obtained from an undistorted surface (i.e., interlayer spacing equal to the bulk value 1.43 Å). In curve (b) the outer layer is contracted by 15% to 1.214 Å, and in curve (e) it is contracted by 20% from the bulk value to 1.142 Å. Curve (d) is computed for incident beam angles $\theta = 5°$ and $\phi = 90°$, which are the same angles as measured for the experimental curve (c). The remaining curves are calculated at normal incidence. The theoretical curves are all shifted by 3.65 eV to account for the metallic work function.

Fig. 17. Diffraction pattern from the Pt(100) crystal face exhibiting the (5×1) surface structure.

Fig. 18. One crystallographic zone of platinum. The points indicate the directions of the various cuts.

Fig. 19. Diffraction pattern and schematic representation of a stepped surface that was cut 6.5° from the (111) crystal face. The notation to identify this surface is Pt(5)-[9(111)×(111)].

Fig. 20. Diffraction pattern and schematic representation of the Pt(S)-[6(111)×(100)] stepped surface.

Fig. 21. Diffraction pattern and schematic representation of the Pt(S)-[5(100)×(111)] stepped surface.

Fig. 22. Diffraction pattern and schematic representation of the Pt(S)-[7(111)×(310)] stepped surface.

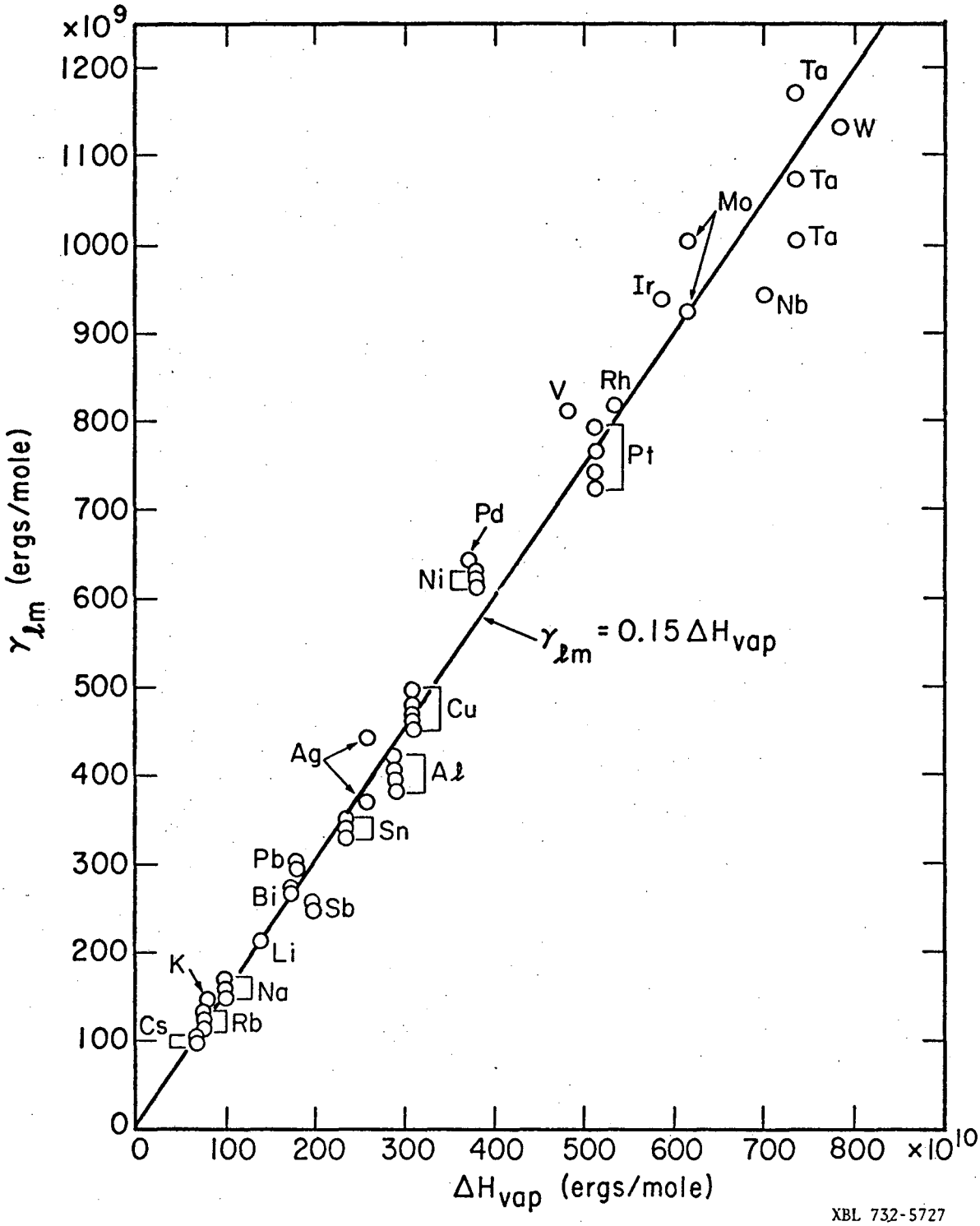
×10^9
1200
1100
1000
900
800
700
600
500
400
300
200
100
0
γℓm (ergs/mole)
0
100
200
300
400
500
600
700
800
×10^10
ΔHvap (ergs/mole)
γℓm = 0.15 ΔHvap
Ta
W
Ta
Mo
Ta
Ir
Nb
V
Rh
Pt
Pd
Ni
Cu
Ag
Aℓ
Sn
Pb
Bi
Sb
Li
K
Na
Rb
Cs
XBL 732-5727

Fig. 1

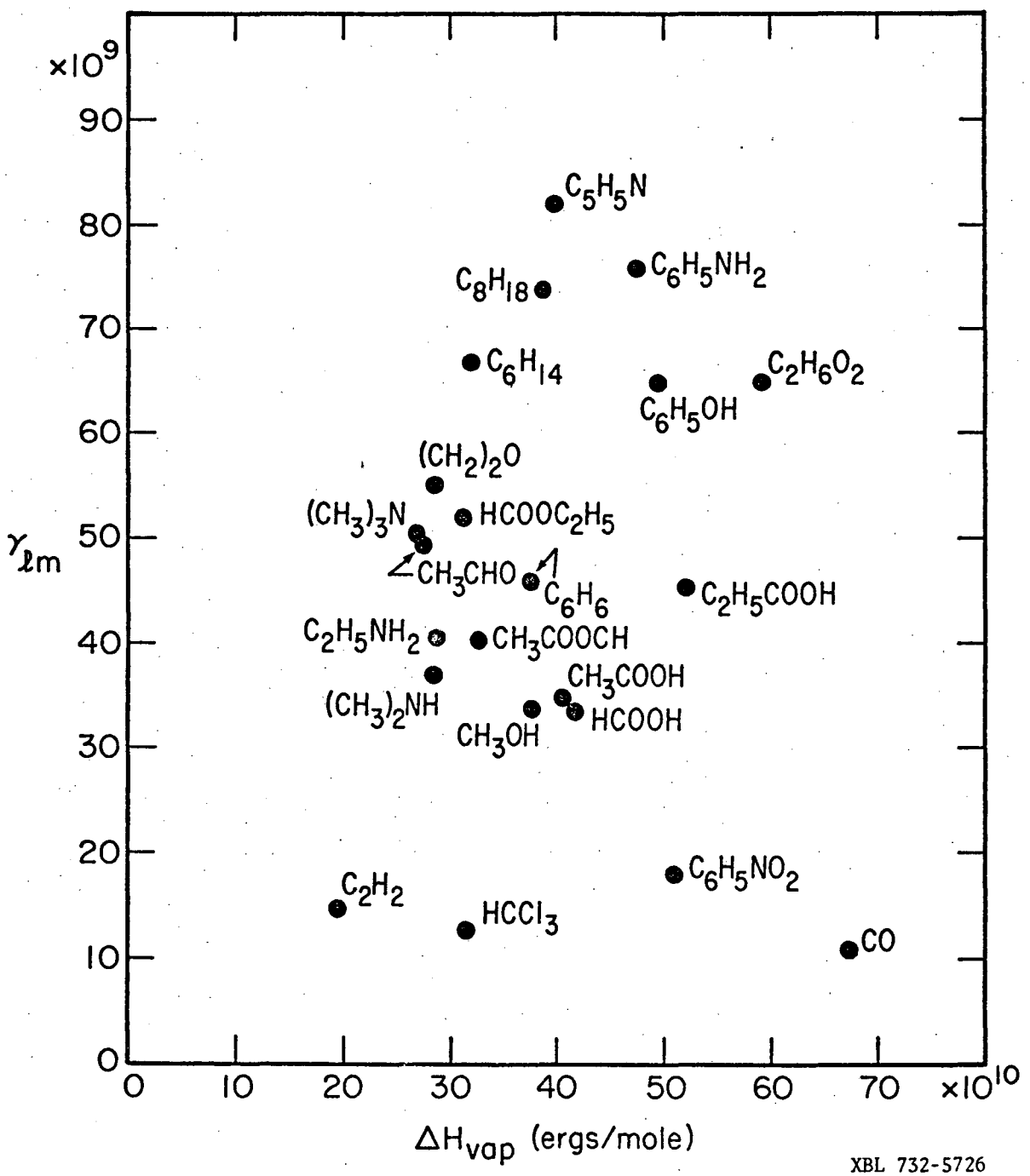
×10^9
90
80
70
60
50
40
30
20
10
0
γℓm
C5H5N
C6H5NH2
C8H18
C6H14
C2H6O2
C6H5OH
(CH2)2O
(CH3)3N
HCOOC2H5
CH3CHO
C6H6
C2H5COOH
C2H5NH2
CH3COOCH
CH3COOH
(CH3)2NH
HCOOH
CH3OH
C6H5NO2
C2H2
HCCl3
CO
0
10
20
30
40
50
60
70
×10^10
ΔHvap (ergs/mole)
XBL 732-5726

Fig. 2

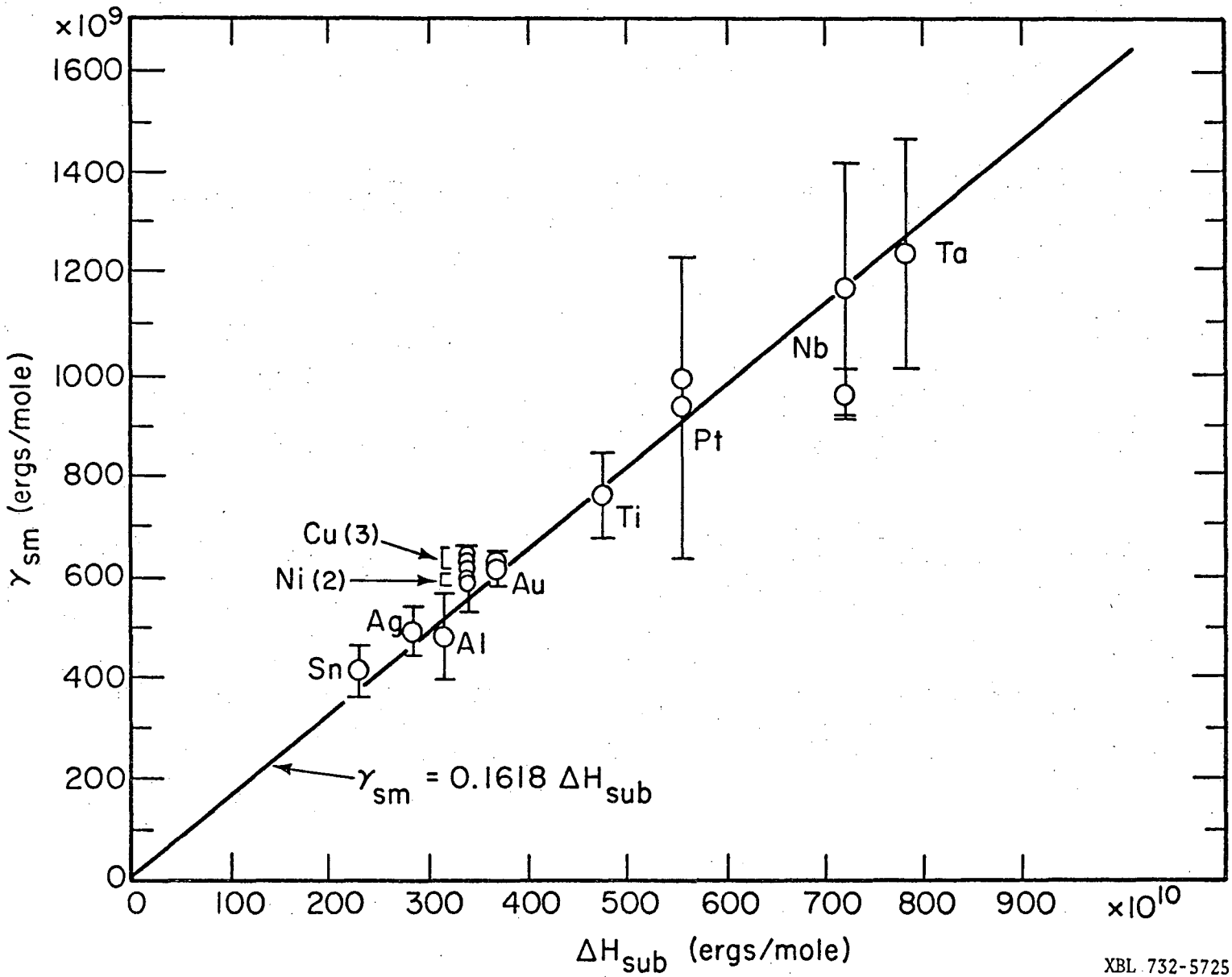
×10^9
1600
1400
1200
1000
800
600
400
200
0
γsm (ergs/mole)
0
100
200
300
400
500
600
700
800
900
×10^10
ΔHsub (ergs/mole)
Cu (3)
Ni (2)
Au
Ag
Al
Sn
Ti
Pt
Nb
Ta
γsm = 0.1618 ΔHsub
XBL 732-5725

Fig. 3

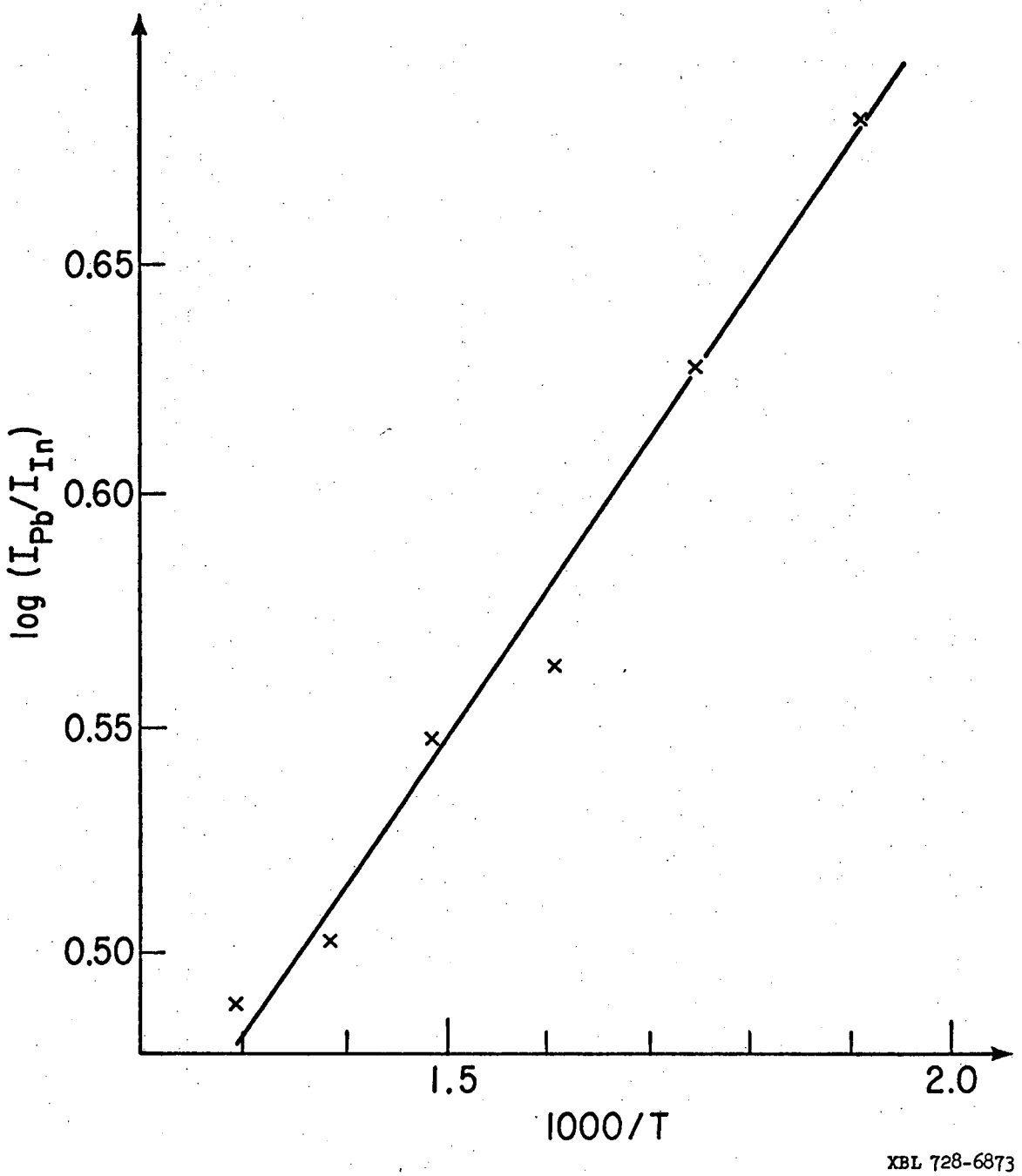


Fig. 4

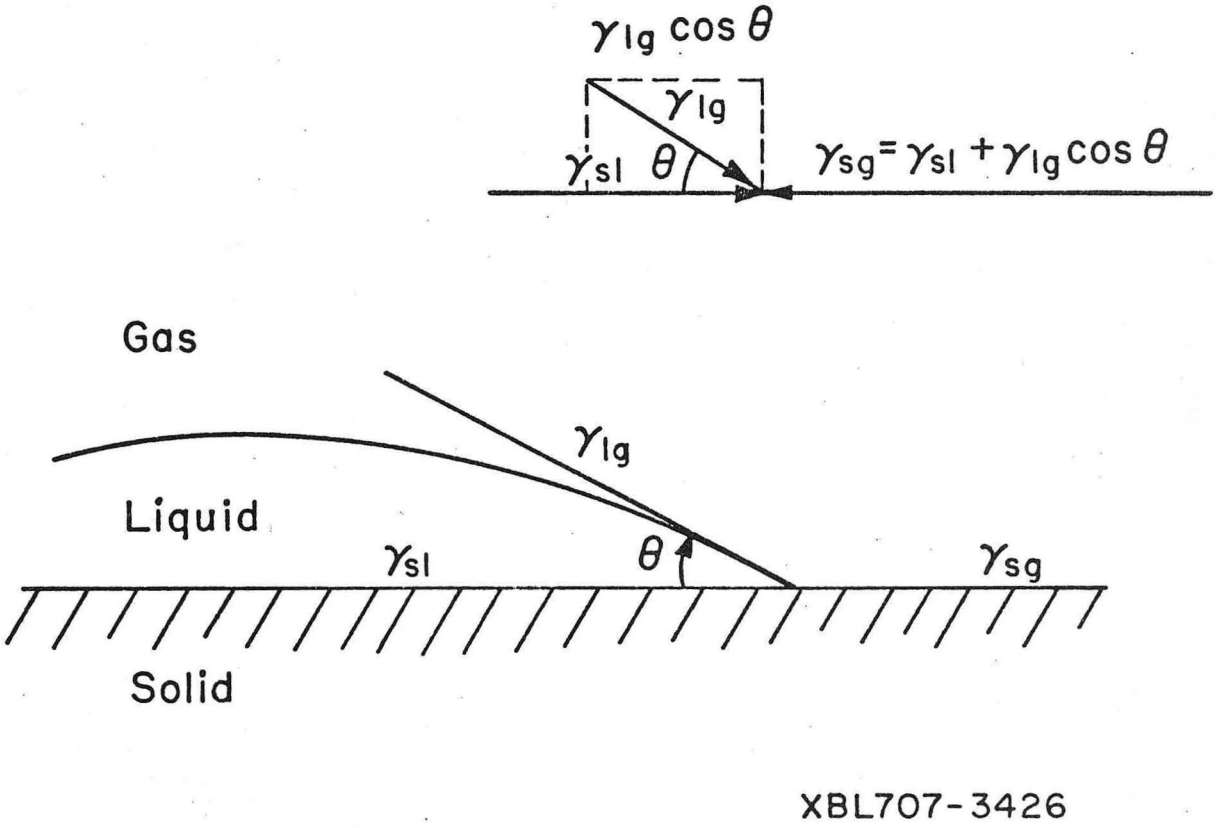
$\gamma_{lg} \cos\theta$
$\gamma_{lg}$
$\gamma_{sl}$
$\theta$
$\gamma_{sg} = \gamma_{sl} + \gamma_{lg} \cos\theta$
Gas
$\gamma_{lg}$
Liquid
$\gamma_{sl}$
$\theta$
$\gamma_{sg}$
Solid
XBL707-3426

Fig. 5

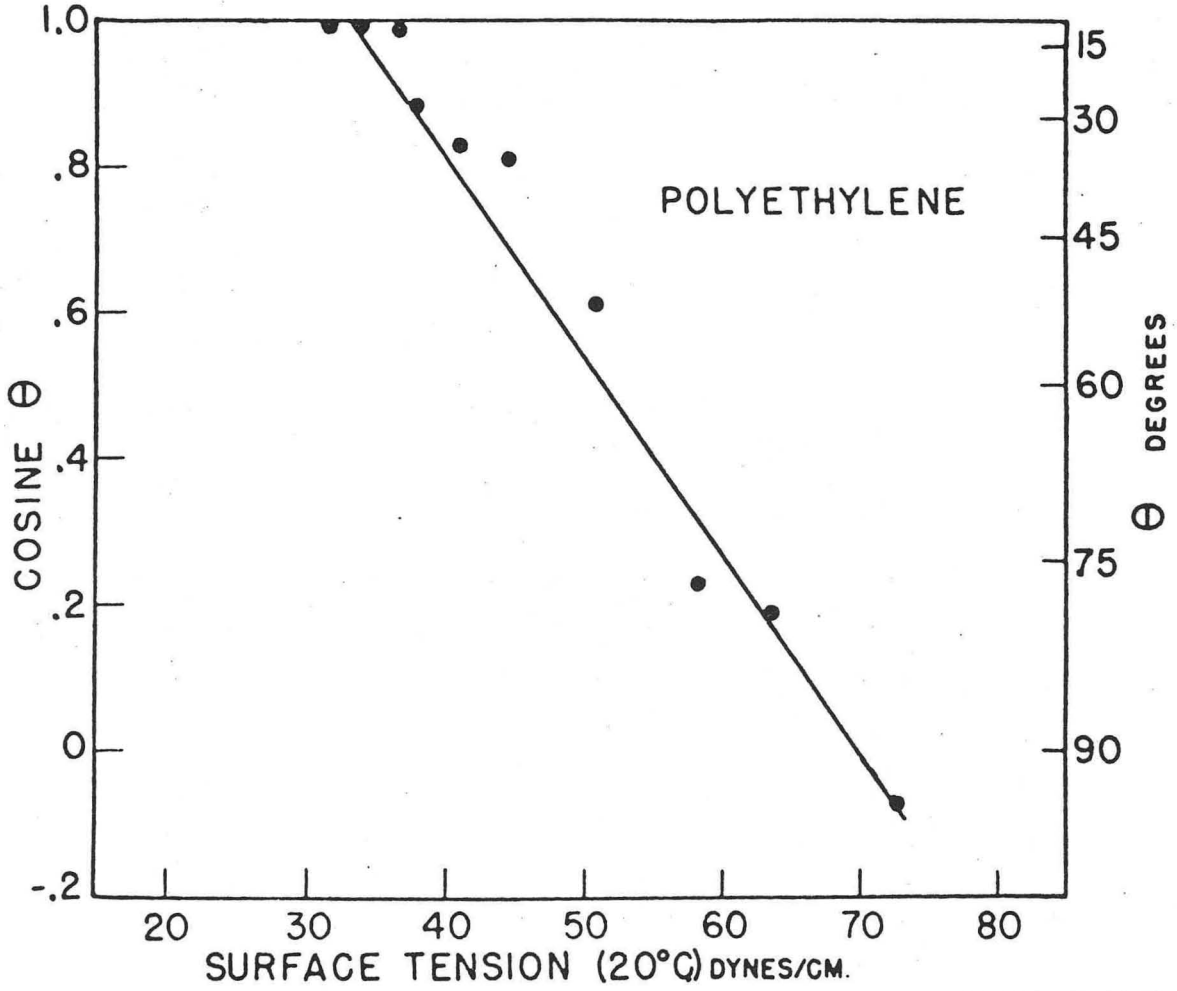


XBL 7310-1933

Fig. 6

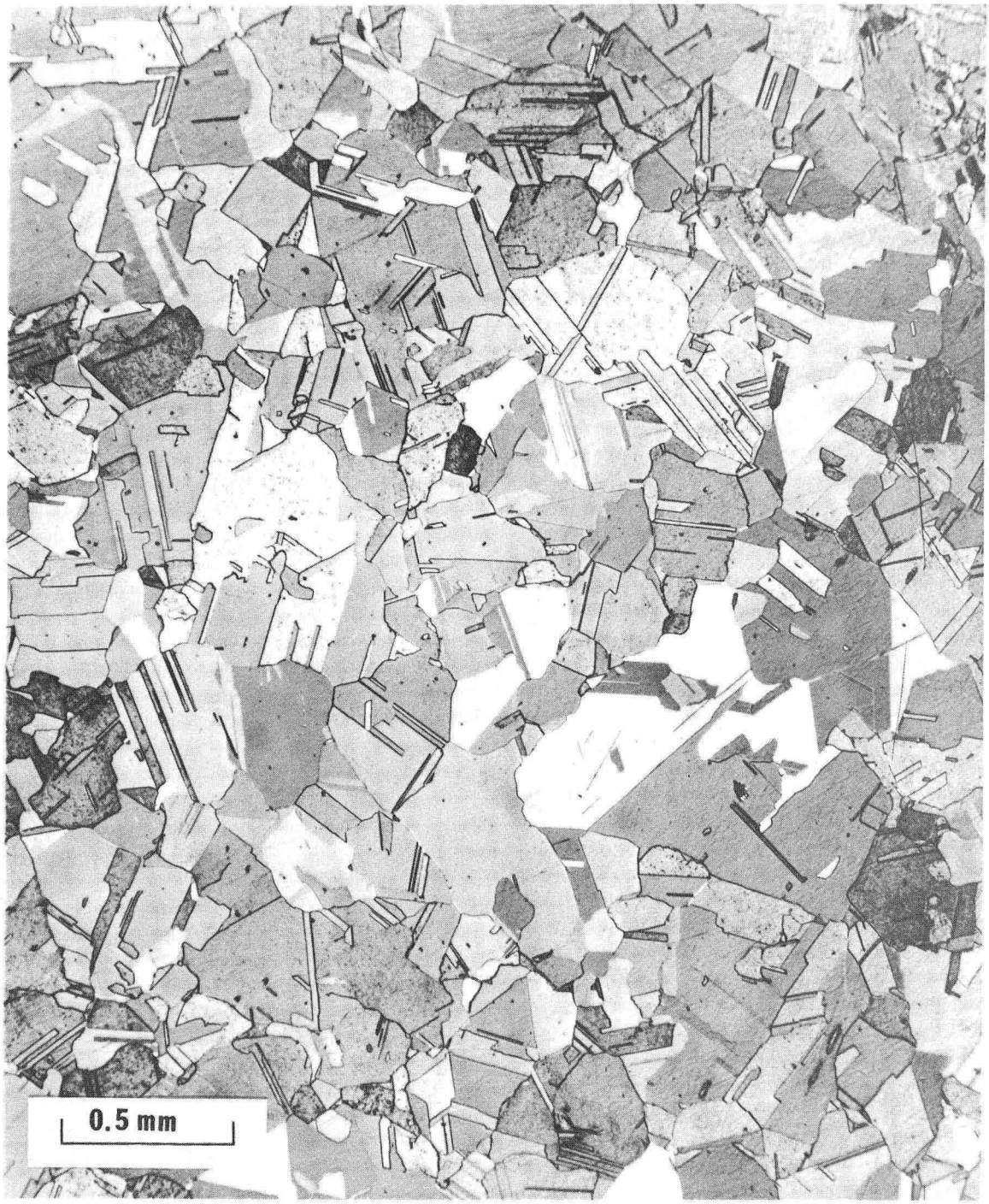


XBB 7310-6331

Fig. 7

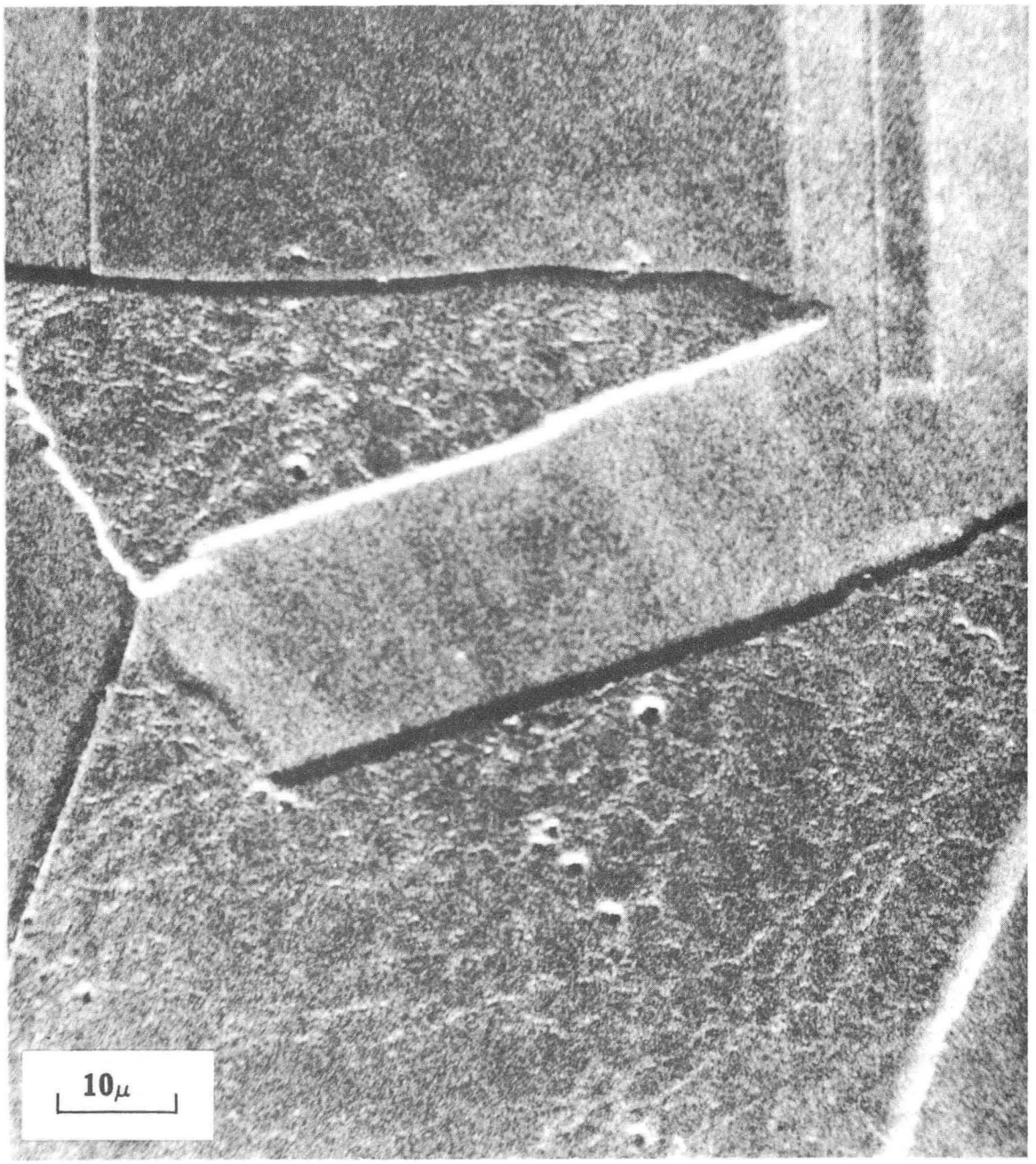


XBB 7310-6330

Fig. 8

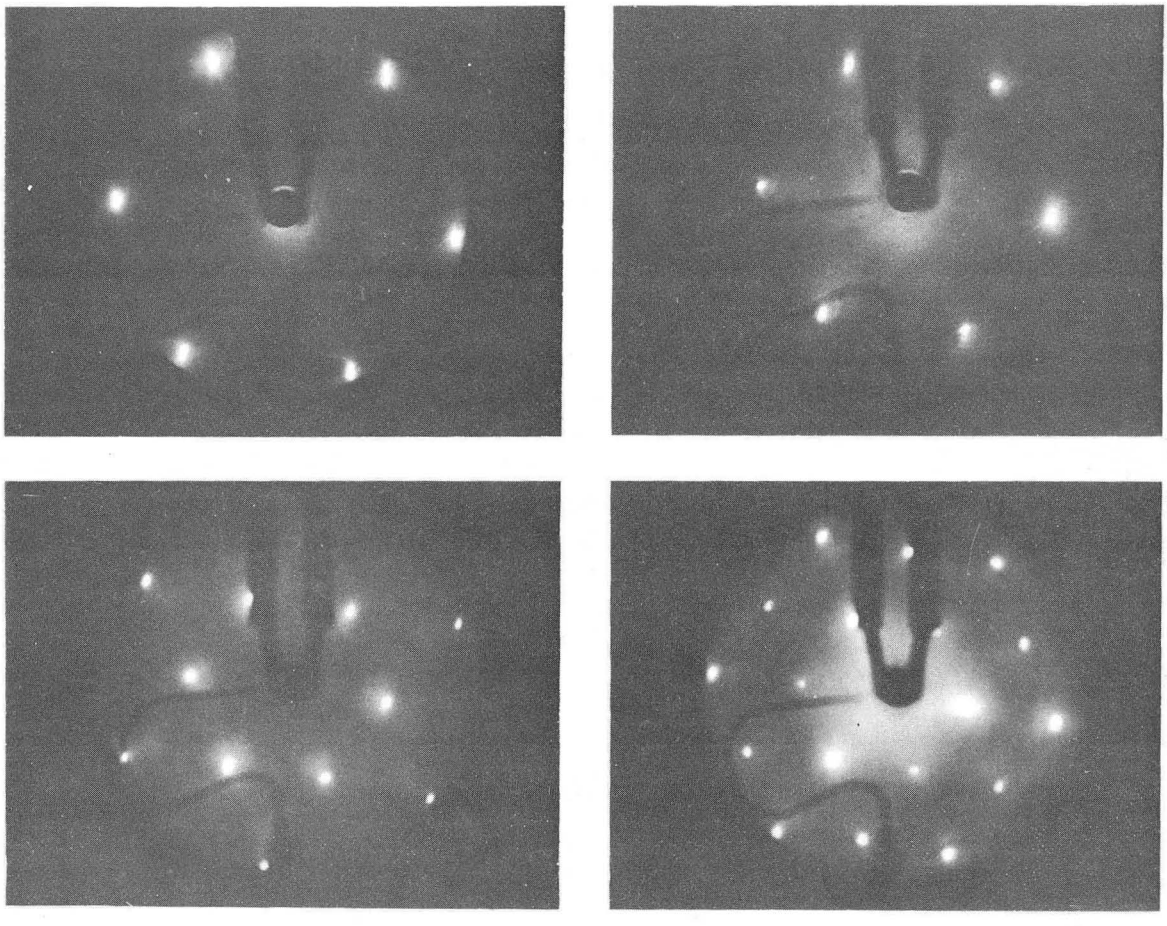

XBB 7012-5685

Fig. 9

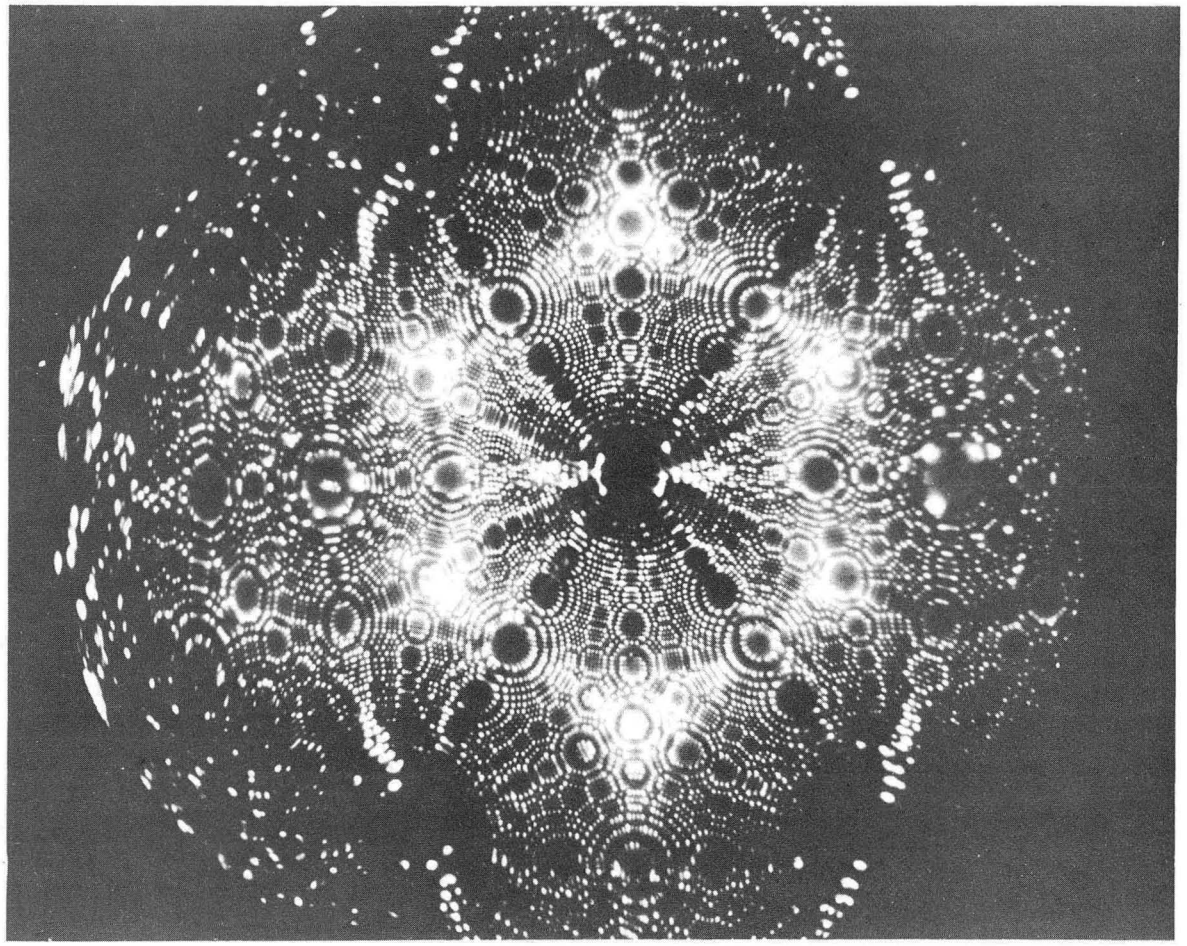

XBB 7310-6332

Fig. 10

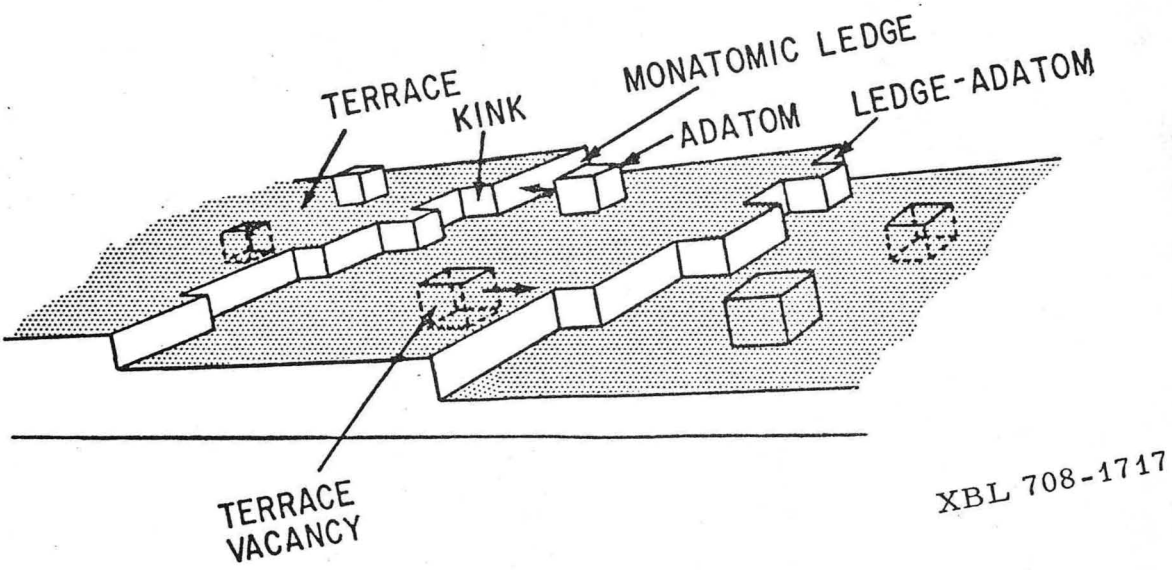


XBL 708-1717

Fig. 11

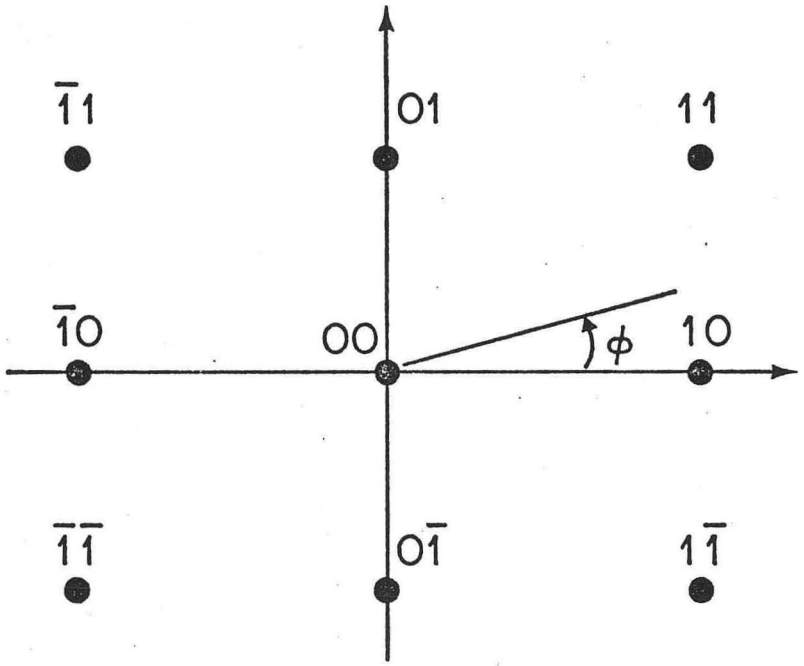


Fig. 13

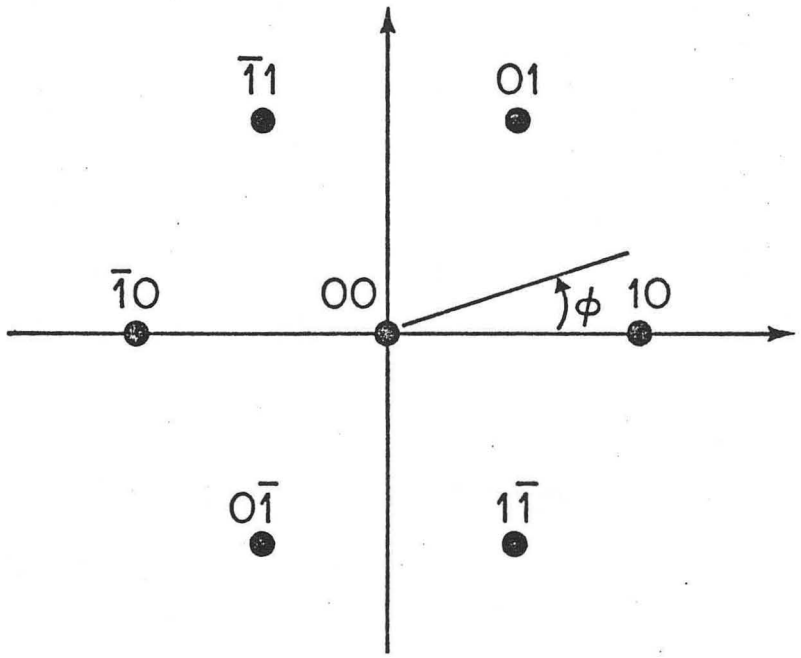


Fig. 12

XBL728-6877

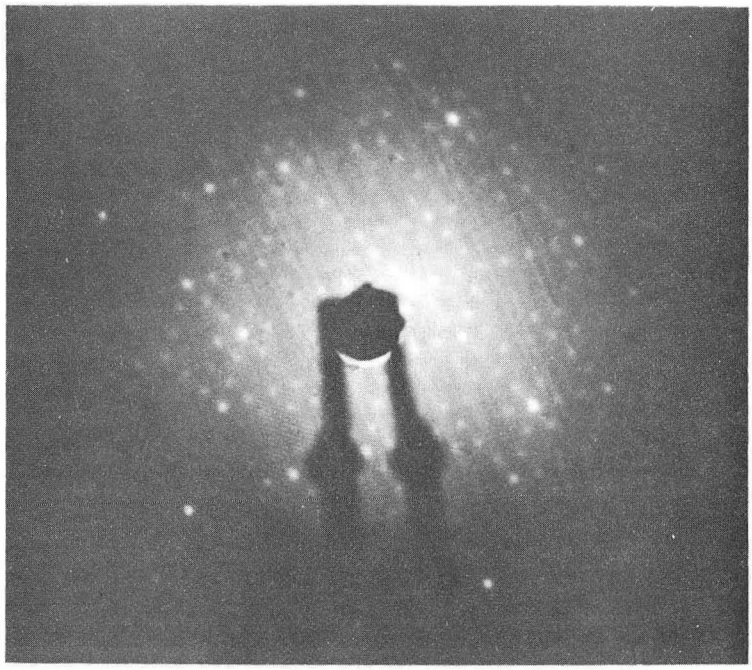

a

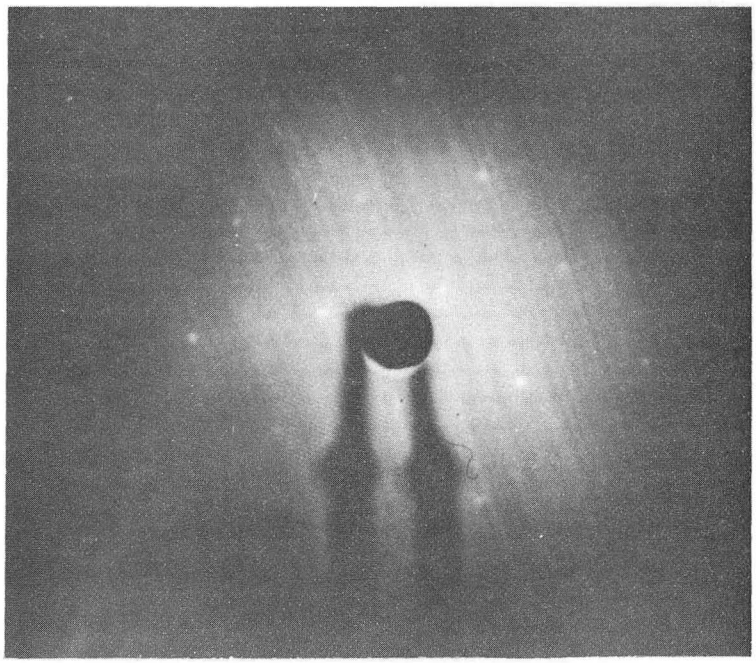

b

XBB 6911-7077

Fig. 14

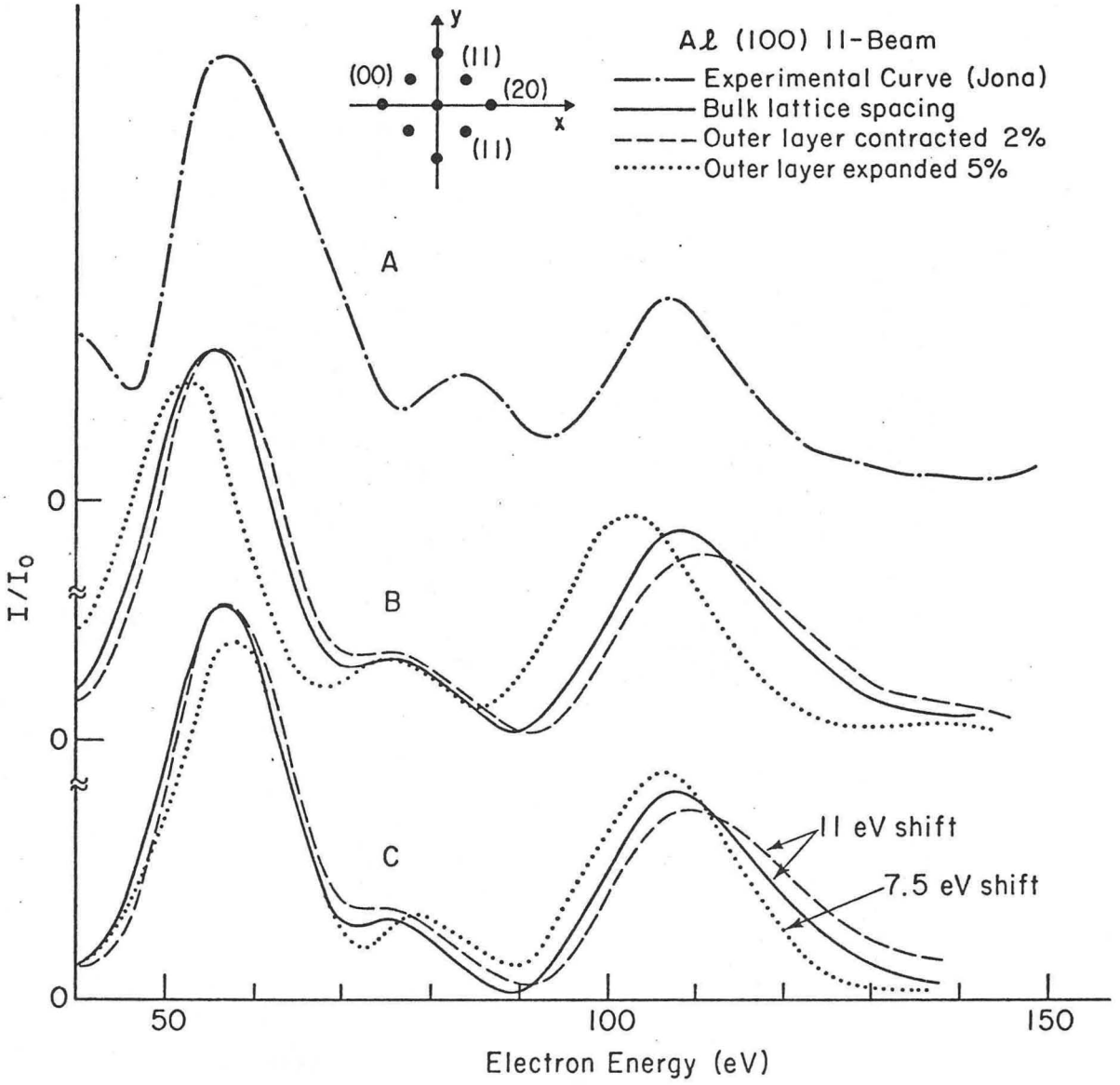


XBL 727-6583

Fig. 15

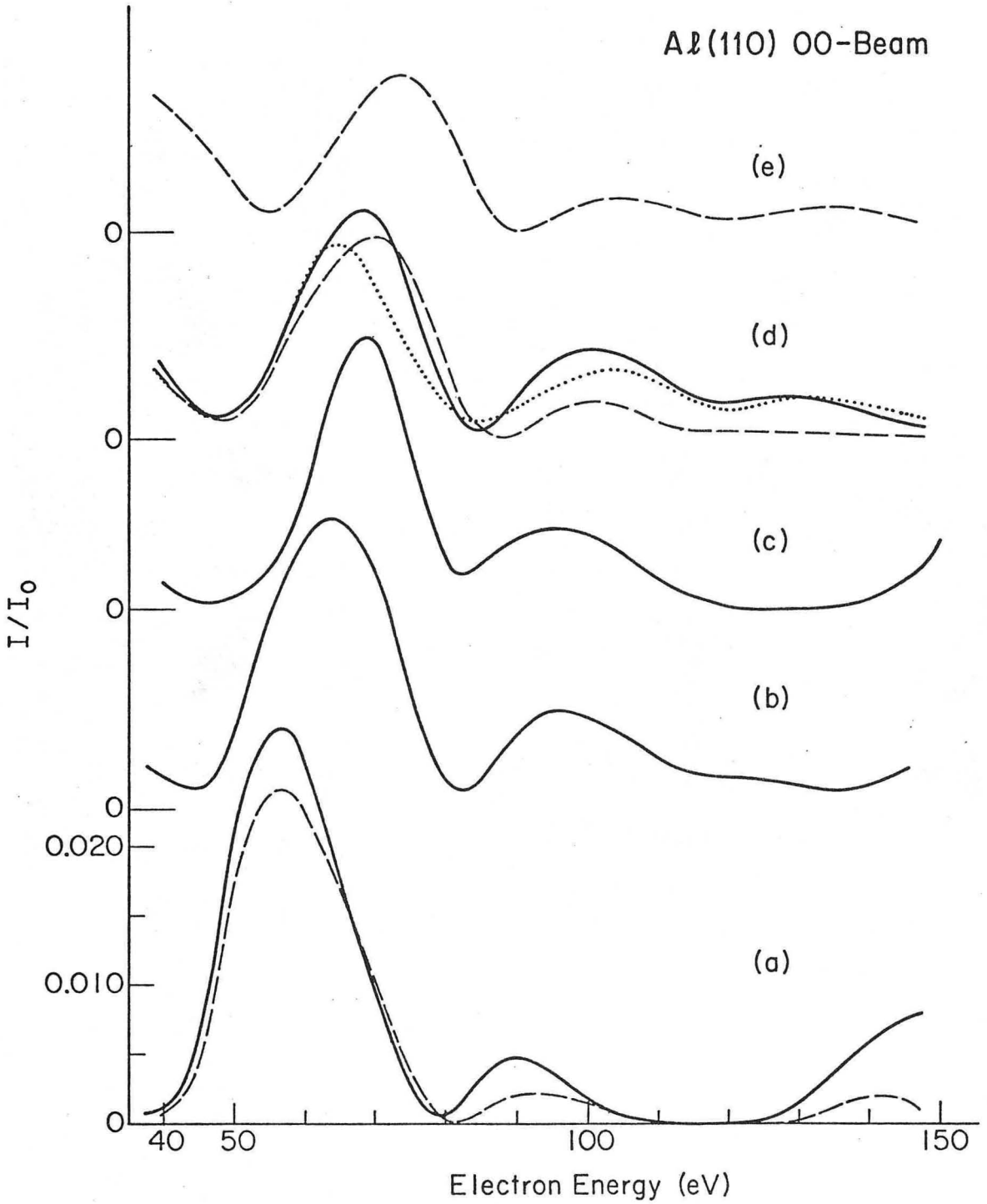


XBL728-6797

Fig. 16

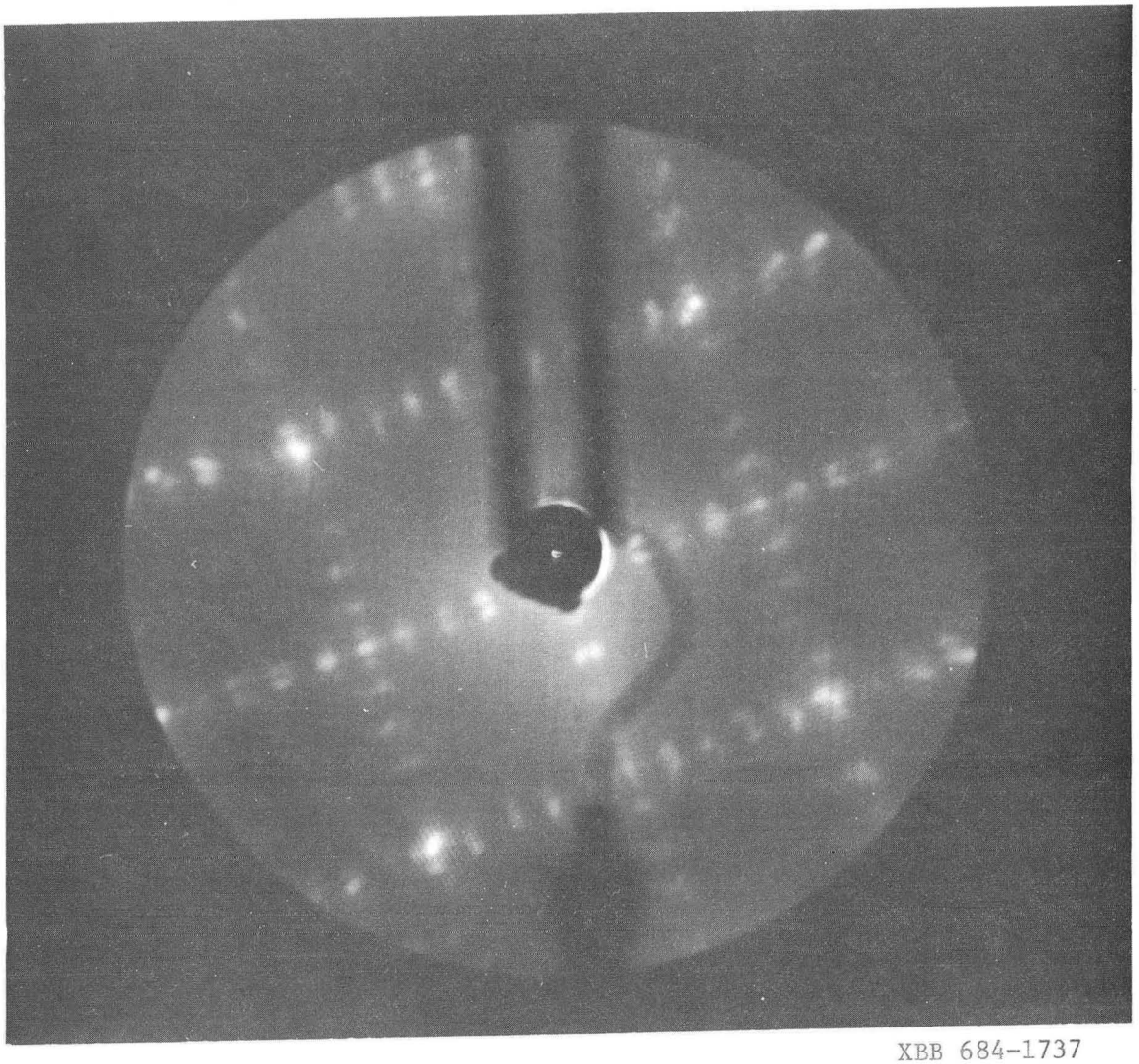

XBB 684-1737

Fig. 17

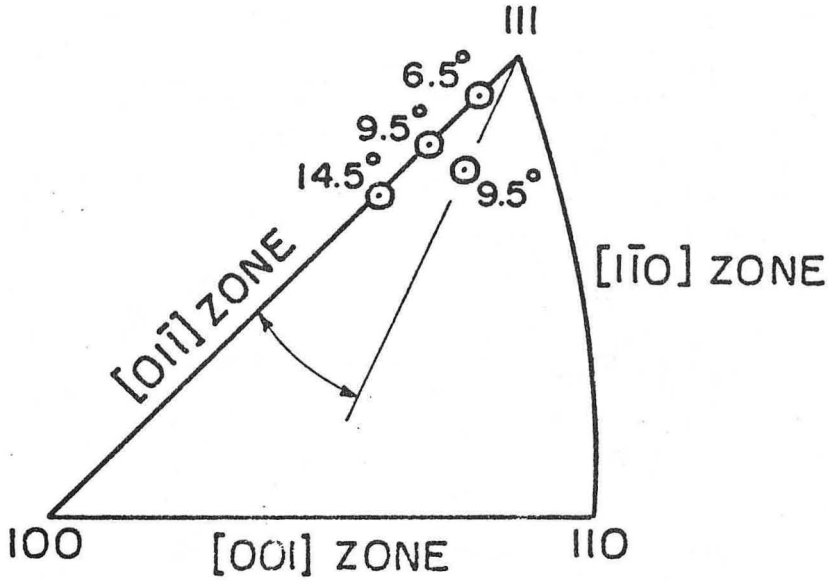


XBL 733-5906

Fig. 18

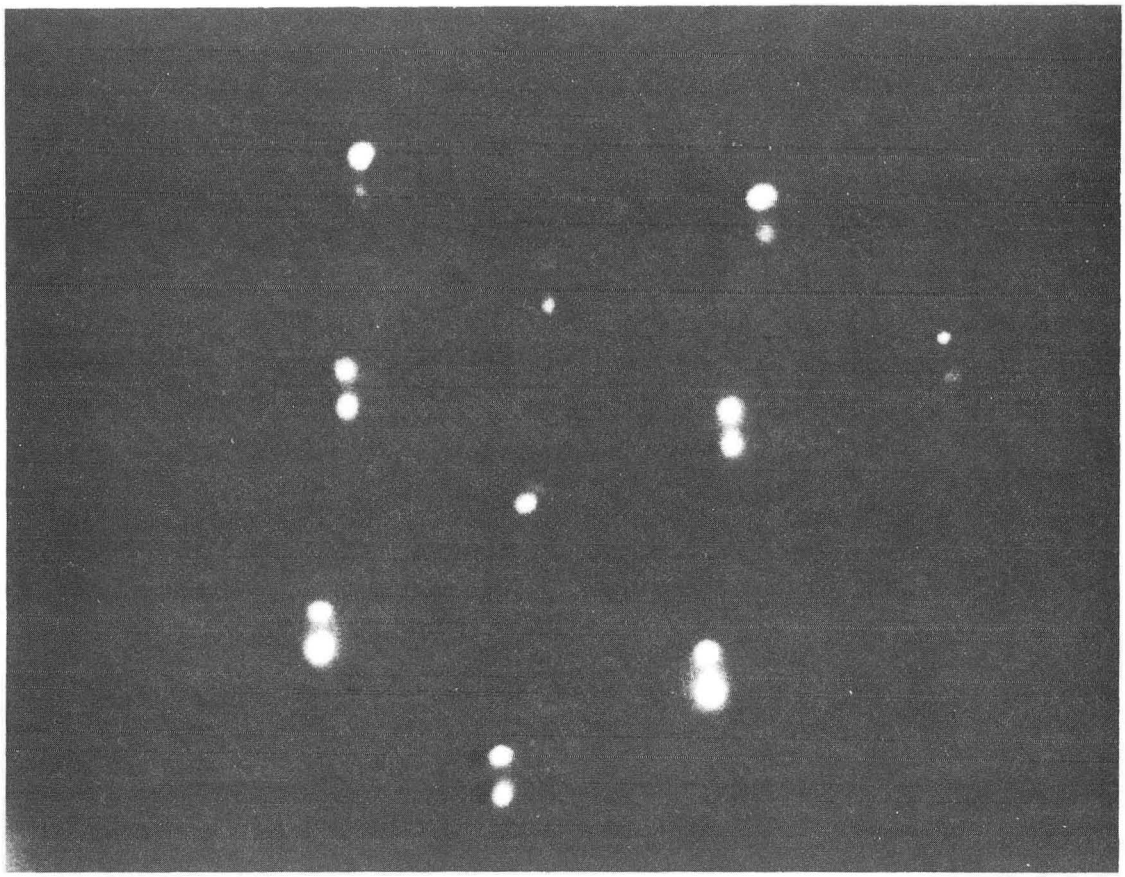

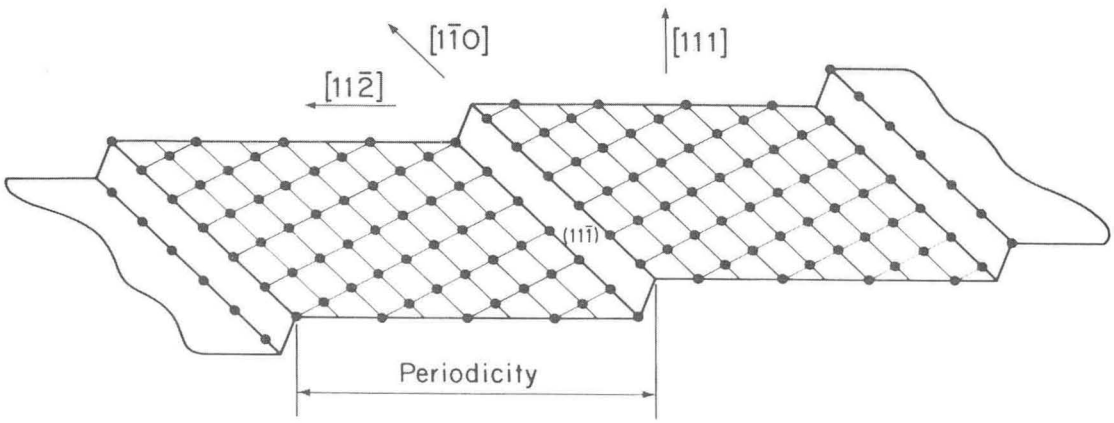


XBB 739-5422

Fig. 19

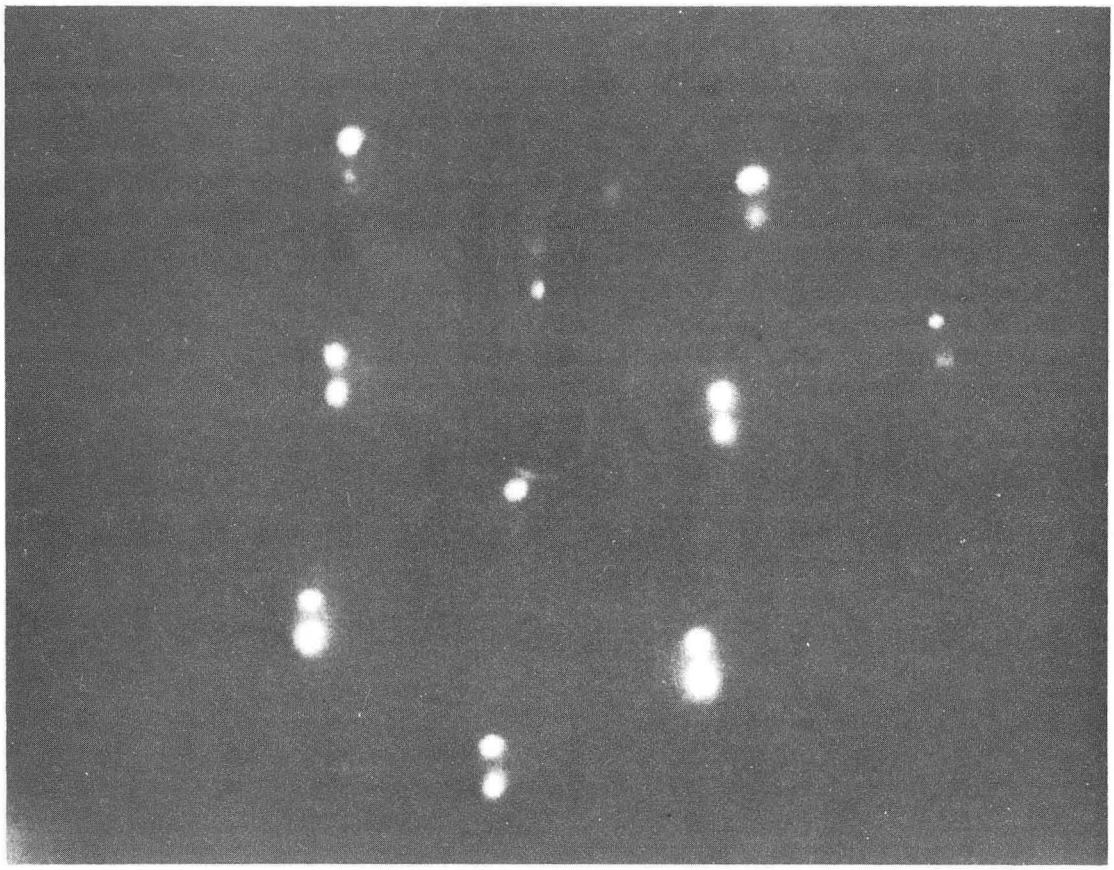

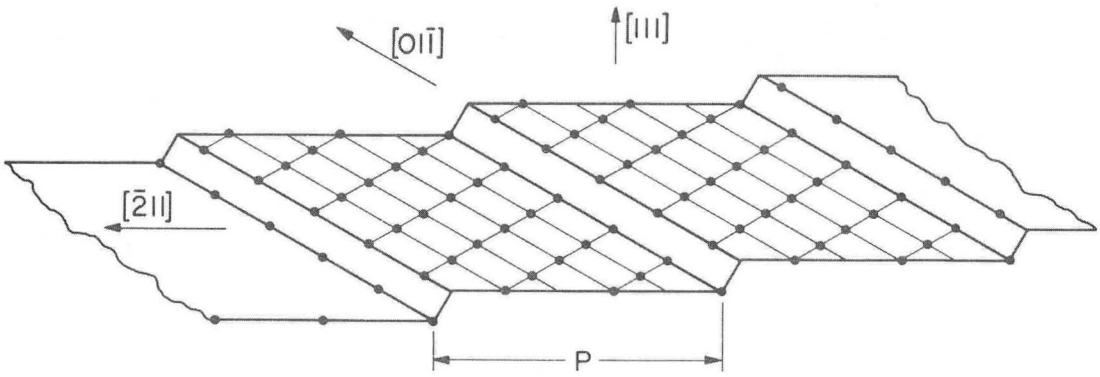


XBB 733-2083

Fig. 20

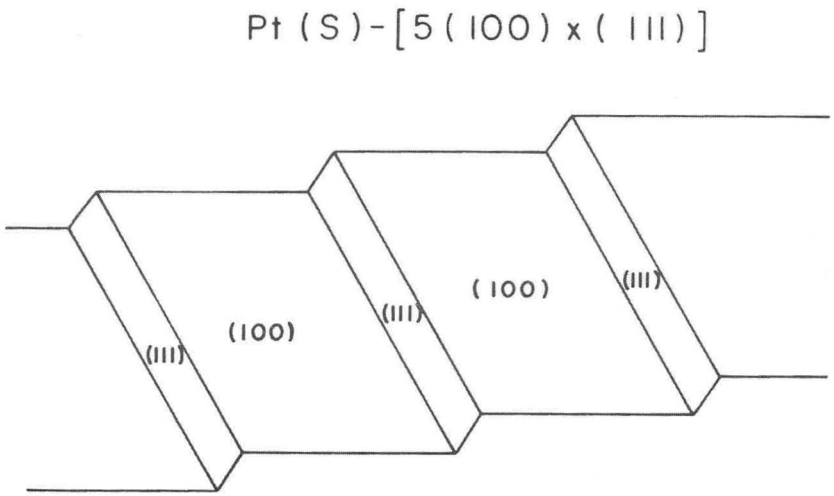


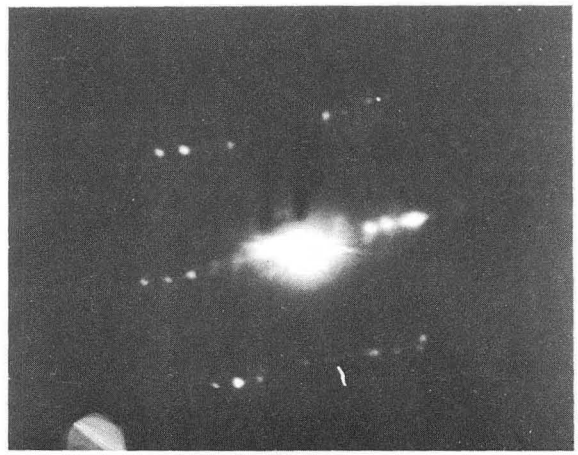

XBB 7111-5365

Fig. 21

P+(S)-[7(111)X(310)]

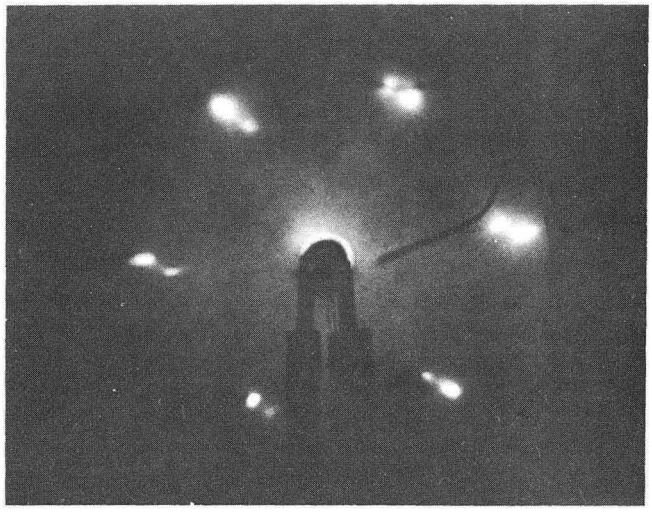

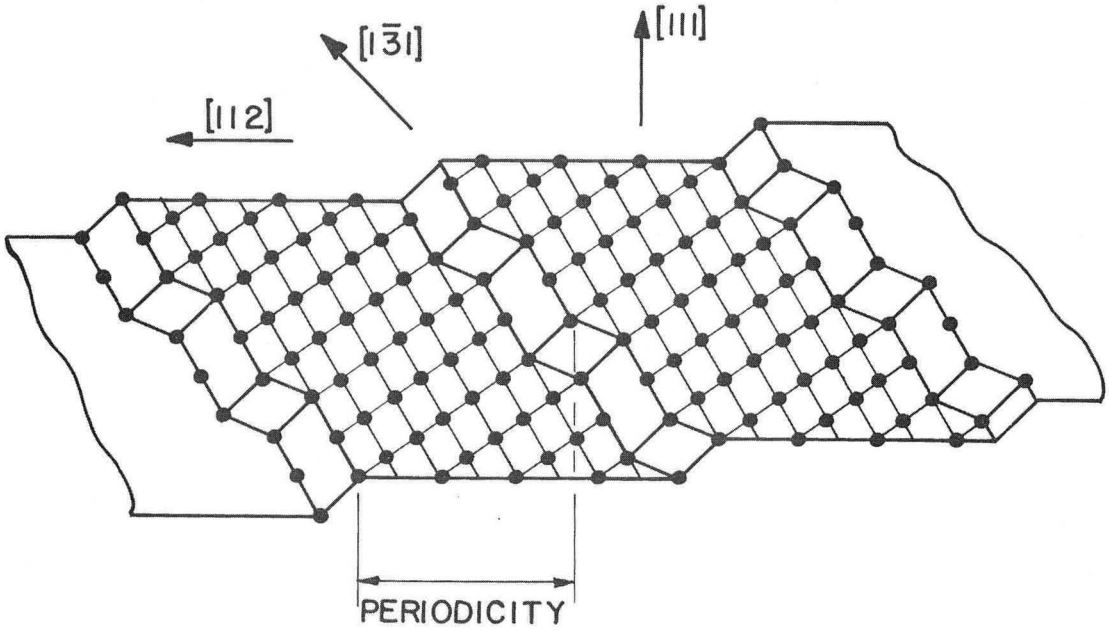


XBB 733-2189

Fig. 22

LEGAL NOTICE

*This report was prepared as an account of work sponsored by the United States Government. Neither the United States nor the United States Atomic Energy Commission, nor any of their employees, nor any of their contractors, subcontractors, or their employees, makes any warranty, express or implied, or assumes any legal liability or responsibility for the accuracy, completeness or usefulness of any information, apparatus, product or process disclosed, or represents that its use would not infringe privately owned rights.*

*TECHNICAL INFORMATION DIVISION*
*LAWRENCE BERKELEY LABORATORY*
*UNIVERSITY OF CALIFORNIA*
*BERKELEY, CALIFORNIA 94720*